ARTICLE

https://doi.org/10.1590/2317-4889202120200119

BJGEO
Brazilian Journal of Geology

The origin of supergene nickeliferous chlorite in the Santa Fé Ni-Laterite Deposit, GO, Brazil

Matheus Lamas Machado[1]*, Claudio Gerheim Porto[1], Licia Santoro[2], Francesco Putzolu[3], Reiner Neumann[4], Artur Bastos Neto[5], Helena Polivanov[1], Richard Herrington[2]

Abstract

The Santa Fé Ni laterite deposit (Brazil) developed as a consequence of weathering of serpentinized dunites that produced a regolith in which the main Ni ore zone is a ferruginous saprolite with chlorite as the main ore-carrier along with Ni-bearing Fe-oxyhydroxides. The genesis of chlorite is related to hydrothermal alteration of spinel. This study found that part of the chlorite has a supergene origin. XRPD-Rietveld method and EMPA/SEM analyses coupled with geochemical and mass balance calculations have provided further information about the chemistry and mineralogy of the main ore minerals. An attempt is made to explain the mode of formation of secondary chlorite and associated ore minerals. The main Ni-bearing minerals in the green saprolite are serpentine and minor chlorite. In the ferruginous and ochreous saprolites chlorite is a major phase with Ni contents of the order of 3 and 7 wt% NiO, respectively. Fe-oxy-hydroxides (mean NiO = 1.8 wt%) are also abundant in the ferruginous and ochreous saprolites. According to the isocon method, Al and Ti are definitely enriched in the saprolite compared to dunite. The source of Al for chlorite formation probably derives from pyroxenites and peridotite. The lateral migration of Al in solution was fundamental for the supergene formation of chlorite.

KEYWORDS: nickeliferous chlorite; Ni-laterite; mass balance; Santa Fé; Brazil.

INTRODUCTION

Nickel laterites are supergene regolith-hosted deposits formed from the alteration of ultramafic rocks (*e.g.* peridotites, dunites, etc.), where fosteritic olivine and/or serpentine are the main Ni sources during the weathering process (Butt and Cluzel 2013). The ideal conditions under which these deposits form depend on the combined effect of several factors such as tectonic setting, morphoclimatic regime, drainage network, chemistry of groundwater and time (Golightly 1981, 2010, Elias 2002, Gleeson *et al.* 2003, Freyssinet *et al.* 2005, Porto 2016). The formation of Ni-laterites is favored in tropical climatic regimes, thus most modern laterites are located near the tropical zone (Elias 2002, Butt and Cluzel 2013). Common tectonic settings in which Ni-laterites occur are: ultramafic rocks in ophiolitic complexes (Cuba, Indonesia); and cratonic platforms in association with mafic-ultramafic intrusions (Central Brazil, Australia) (Freyssinet *et al.* 2005).

Three Ni-laterite groups have been described according to their dominant Ni mineralogy and regolith profile structure (Brand *et al.* 1998, Elias 2002, Butt and Cluzel 2013): in the hydrous Mg-silicate type, the main Ni-bearing minerals belong to the garnierite group, which is a complex mixture of Mg-hydrous phyllosilicates (Ni-rich serpentines with talc, chlorite, and smectite). The main ore zone of this deposit type is located in the lower portions of the regolith (saprolite zone), where garnierite occurs as vein fillings in fractures and open spaces. Golightly (2010) associates this type of deposit to permanently wet rainforest setting in a tectonically active terrane with moderate relief. In the clay silicate type, the ore zone occurs in the plasmic horizon of the saprolite and consists of Ni-bearing smectite clays (*e.g.* nontronite, saponite, montmorillonite, etc.). According to Golightly (2010), this type is associated with a morphoclimatic setting dominated by peneplains under an increasingly arid regime. The type locality of these deposits is represented by the Ni laterite deposits of the Yilgarn Craton in Western Australia. In the oxide-type deposits, Ni is concentrated in Fe- and Mn-oxy-hydroxides occurring in the upper parts of the lateritic profile. Furthermore, in these oxide-type deposits, Mn-oxy-hydroxides play a primary role also in defining the Co deportment (Lambiv Dzemua *et al.* 2013, Putzolu *et al.* 2018).

Central Brazil is home to many relevant Ni-laterite deposits, *i.e.*, Barro Alto, Niquelândia and the deposits of the Santa Fé district, in Goiás State. Carvalho e Silva and Oliveira (1995) and Golightly (2010) proposed that the aforementioned deposits

[1]Universidade Federal do Rio de Janeiro – Rio de Janeiro (RJ), Brazil. E-mails: mattlamachado@gmail.com, porto@geologia.ufrj.br, hpolivanov@gmail.com

[2]Earth Sciences Department, Natural History Museum, Cromwell Road – London, United Kingdom. E-mails: licia.santoro85@gmail.com, r.herrington@nhm.ac.uk

[3]Università di Napoli "Federico II" Complesso Universitario di Monte S. Angelo – Napoli, Italy. E-mail: francescoputzolu91@libero.it

[4]Centro de Tecnologia Mineral, Ministério da Ciência, Tecnologia e Inovações – Rio de Janeiro (RJ), Brazil. E-mail: reiner.neumann@gmail.com

[5]Instituto de Geociências, Universidade Federal do Rio Grande do Sul – Porto Alegre (RS), Brazil. E-mail: artur.bastos@ufrgs.br

*Corresponding author.

are part of dissected peneplains that have undergone climatic regimes ranging from arid to permanently wet. This category also includes the Ni-laterite deposits of the Carajás Province and the adjacent Araguaia belt (Paixão *et al.* 2008). Niquelândia and Barro Alto have the main ore phases as garnierite and smectite clays, developed over a narrow elongated Archean to Early Proterozoic layered ultramafic intrusion, comprising partially serpentinized peridotites and pyroxenites (Colin *et al.* 1990, Carvalho e Silva e Oliveira 1995). In Santa Fé, the laterite profile developed over an Upper Cretaceous ultramafic intrusion, predominantly consisting of serpentinized dunites, and is characterized by a well-developed oxide zone, where the economic concentration of Ni ore is observed.

The Santa Fé deposit was discovered in the 1970s; it was first studied by Barbour (1976), Oliveira and Melfi (1979), Oliveira and Trescases (1980), Barbour and Hypolito (1983), and was later reviewed by Carvalho e Silva and Oliveira (1995). Exploration work was reinitiated in the early 2000s with intensive drilling, which produced a large amount of new data that were further studied by Golightly (2010) and Putzolu *et al.* (2021).

Putzolu *et al.* (2021), by means of geochemical and mineralogical analyses, have identified that, rather unusually, Ni-rich chlorite occurs throughout the lateritic profile. To explain its occurrence, the authors above proposed that chlorite formation was triggered by the hydrothermal alteration from chromite to ferritchromite. In a SiO_2-saturated system, this process could have supplied the suite of elements (Al, Cr, Mg, and Si) necessary for chlorite formation. They have also proposed that, during the alteration, part of Co was concentrated in secondary spinels, which could potentially lead to the refractory behavior of Co during metallurgical processing.

However, it is also possible that part of the Ni-rich chlorite present in the regolith may have experienced supergene overprinting. Therefore, further investigations were conducted through the reinterpretation of whole-rock geochemical data; mineral chemistry analysis using Scanning Electron Microscopy (SEM) and Electron Microprobe Analysis (EMPA); quantitative mineralogy by the Rietveld method of refinement of X-ray powder diffraction (XRPD) patterns; and application of mass balance techniques. With this approach in mind, this study aimed to explain the origin of Ni-rich chlorite and associated ore minerals in the regolith.

GEOLOGICAL SETTING

The Ni-laterite deposit of Santa Fé is situated 5 km NW of the Santa Fé village in the southwestern part of Goiás State, Central Brazil (Fig. 1A). The laterite ore developed over the Santa Fé ultramafic massif, which is part of the Goiás Alkaline Province (GAP) (Almeida 1967, Brod *et al.* 2005). The GAP is part of the Cretaceous alkaline-ultramafic complexes originated from the magmatism related to the opening of the South Atlantic during the Wealdenian Reactivation. This extensional event can be placed in the same tectonic context as the flood basalts of the Serra Geral Formation of the Lower Cretaceous (~120 Ma) (Almeida 1967, Carvalho e Silva and Oliveira 1995). The basement rocks are Middle Ordovician Gneisses of 467±10 Ma (Barbour and Hypolito 1983) and Siluro-Devonian sandstones of the Paraná Basin, which locally reach up to 200 m in thickness in the GAP region (Danni 1994).

The Santa Fé massif is elliptically shaped with a N-S axis of 9.5 km and a W-E axis of 6.5 km, with a resulting area of about 38 km^2. It is a zoned intrusive body consisting of a core of serpentinized dunites (80% of the massif area), bordered by pyroxenites and peridotites (Fig. 1B). Barbour (1976) dated the magmatism of this massif between 74.4 to 88.4 Ma.

Bedrock mineralogy was investigated by Barbour (1976) and Barbour and Hypolito (1983) and, more recently, by Putzolu *et al.* (2021). They have described a magmatic mineral association composed mostly of olivine with minor pyroxene plus chromite, magnetite, ilmenite, perovskite, and apatite. The later hydrothermal phase overprinted the former assemblage, leading to serpentinization and silicification and to the formation of ferritchromite, vermiculite veins with minor chlorite, carbonates, and amphiboles.

GEOMORPHOLOGY

The geomorphological evolution of Central Brazil was first studied by Braun (1970), who extended the work of King (1956) from SE Brazil to Central Brazil. These authors identified two main erosional surfaces, which were related to two geomorphological cycles. The older *Sul Americana* surface was developed during the Lower Eocene, possibly under relatively more arid conditions than the current ones, leading to extensive silcrete formation (Golightly 1981, 2010, Nahon and Tardy 1992, Carvalho e Silva and Oliveira 1995). Ni-laterite deposits associated with remnants of that surface are generally situated at high elevations, such as the Barro Alto and Niquelândia deposits in Goiás State and the Vermelho deposit in the Carajás region (Colin *et al.* 1990, Carvalho e Silva and Oliveira 1995). The later *Velhas* geomorphological cycle began in Late Oligocene and developed a pediplane that was lateritized under more humid conditions in middle to late Miocene (Braun 1970). Remnants of that surface are extensively preserved in the landscape with a subtle topographic expression, which has nonetheless developed Ni-laterite deposits such as the ones in the Santa Fé district (Santa Fé, Água Branca, Rio dos Bois, Morro dos Macacos, Morro do Engenho, and Iporá) (Fig. 1A). The geomorphology of the Santa Fé region was first investigated by Melfi *et al.* (1979), who suggested that the leveled lowlands where the deposit is located belong to the *Velhas* Erosion Surface and that the silicified tops of the inselbergs interspersed in the deposit area represent relics of the *Sul Americana* erosion Surface.

LATERITIC PROFILE

The Santa Fé lateritic profile occurs mostly over serpentinized dunites. Oliveira and Trescases (1980) and Carvalho

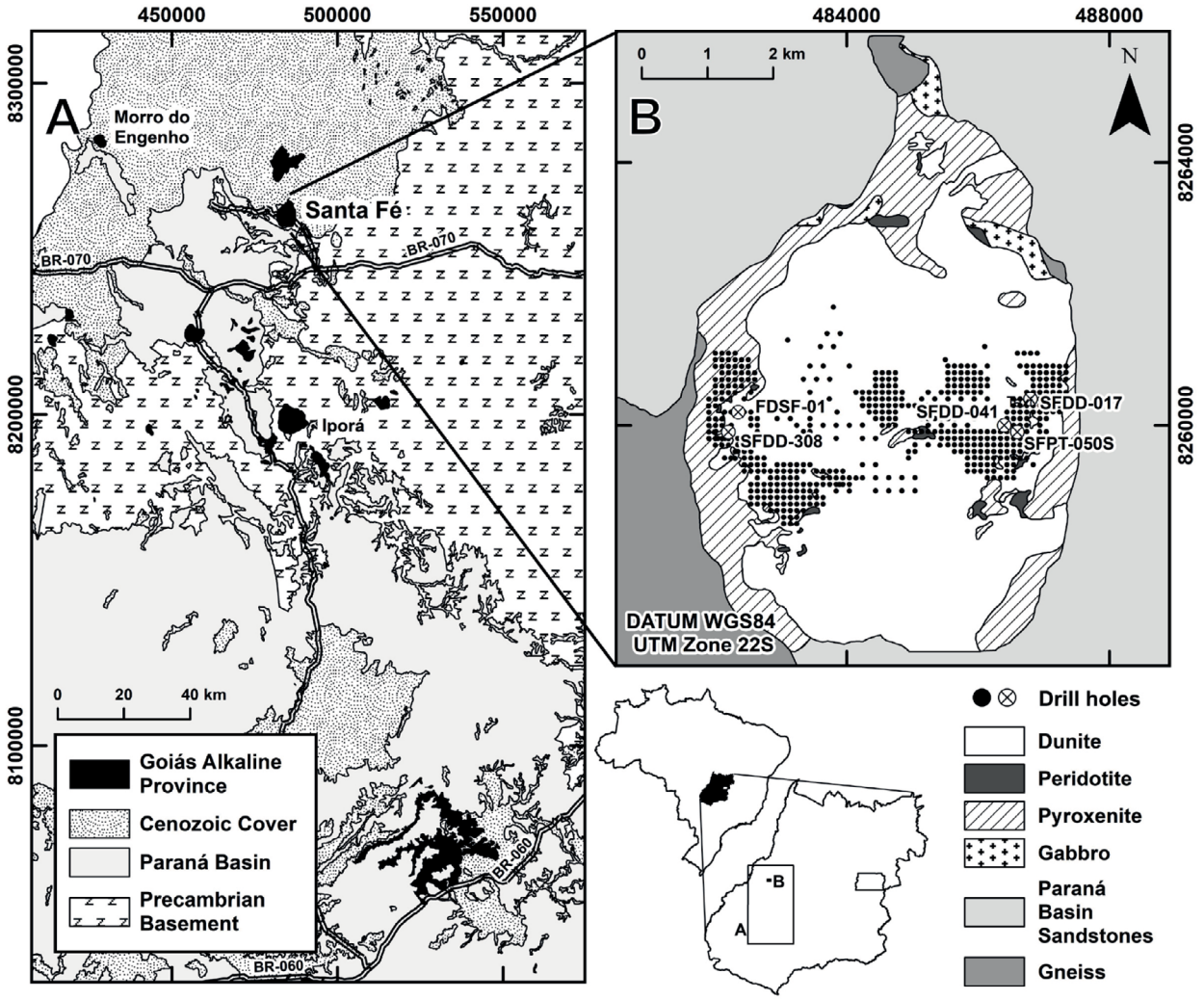

Figure 1. (A) Regional geological map of the Goiás Alkaline Province (GAP) with location of Santa Fé; (B) Geological map of the Santa Fé massif (Barbour and Hypolito 1983), showing the position of 625 selected drill holes grid that generated the geochemical data base used in this work.

e Silva and Oliveira (1995) previously identified four zones, namely: saprock with invariably low Ni grades, rarely exceeding 0.5 wt%; coarse saprolite, with Ni grades varying between 0.3 to 1.3 wt%; ferruginous saprolite, which is the richest in Ni (0.2 to 1.7 wt%); and the top consisting of a red pisolitic material with the lowest Ni grades (up to 0.5 wt%). The lateritic profile developed over peripheral pyroxenites is generally thicker, but the Ni grade is at its minimum.

Putzolu *et al.* (2021) provided more detailed information about the lateritic profile and proposed a new classification of the regolith units, which is adopted in this publication: saprock; saprolite (divided into green, ferruginous, and ochreous); transition zone; and pisolitic soil layer (Fig. 2).

The saprock (avg. thickness = 5 m) is composed mostly of primary minerals in corestones where relict olivine and minor pyroxene are crosscut by extensive serpentine, with minor chlorite and vermiculite micro veinlets along with the hydrothermal phase. Smectite is negligible, but it may occur mostly above the pyroxenitic bedrock as an alteration product of olivine and pyroxene (Oliveira and Melfi 1979). Another common feature of the saprock is the presence of fractures filled by silica and/or carbonates.

The green saprolite (avg. thickness = 2.8 m) is a brownish to greenish clayey unit with minor olivine and pyroxene. Serpentine is still abundant and occurs in two generations: massive and vein-fillings. Remnants of chlorites occur filling cavities in the cryptocrystalline silica or replacing spinel grains. Other minerals include goethite as skeletal aggregates or pseudomorphs after Fe-Mg primary minerals, hematite, magnetite, chromite, and minor smectite. The structures and textures of this unit suggest that it has been formed isovolumetrically (Golightly 1981).

The ferruginous and ochreous saprolites may be locally absent, but where occurring, they add up to 3 m of total thickness to the regolith profile. Goethite is the most abundant phase and is disseminated in the porous matrix, whereas oolitic hematite is more common in the ochreous saprolite. These are the main Ni-bearing units where Ni-rich chlorites and Fe oxy-hydroxides are the main ore minerals. From these units toward the shallower sections of the profile, the saprolite structures and textures may be obliterated by collapse, compaction and/or profile reworking.

A transition zone, where saprolite textures are completely destroyed, leads the way to the pisolitic soil formation (avg.

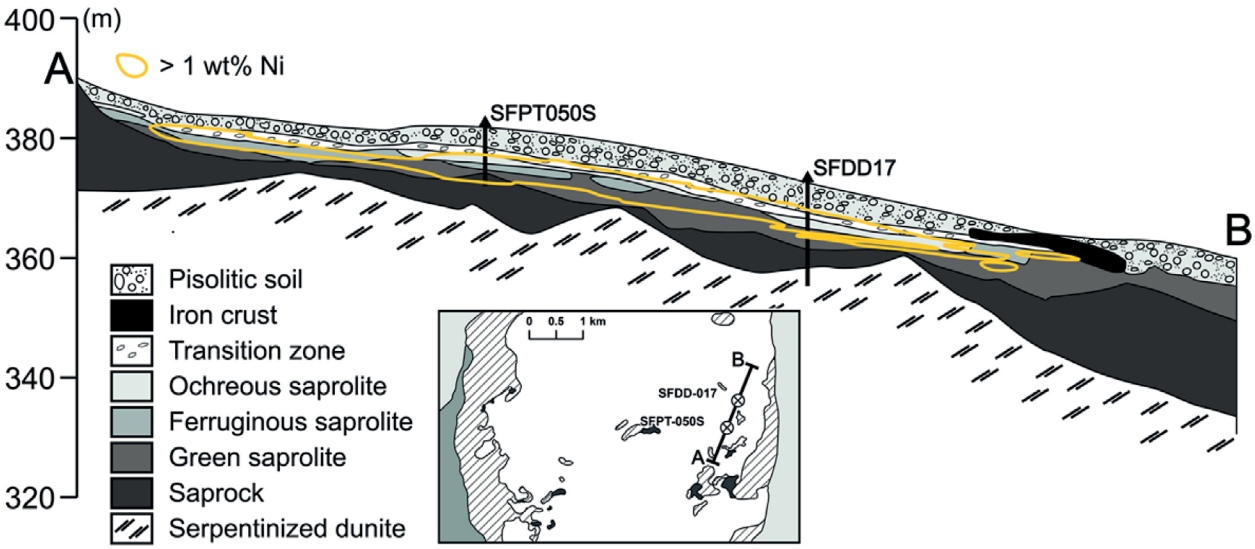

Figure 2. NE-SW cross section passing through SFPT-050S and SFDD-017; mineralized zones with a > 1 wt% Ni grade highlighted in yellow.

thickness = 2.7 m) at the top where hematite is dominant, spinels are residually concentrated and chlorites occur to a lesser extent. At its base a level rich in loose pisolites and oolites set in a ferruginous matrix occurs. This level locally forms a discontinuous lateritic crust, especially in the vicinity of drainage channels. The colluvial nature of the pisolitic soil is suggested by its mode of occurrence, covering the entire area, despite the presence of a lateritic profile unit at depth (Fig. 2).

SAMPLING AND ANALYTICAL TECHNIQUES

Geochemical analysis

Whole-rock geochemical analysis, used for the mass balance study, has been conducted on part of the dataset previously studied by Putzolu *et al.* (2021), which were provided by Teck Cominco Ltda. We selected 8,657 analyses from 535 drill holes performed on the dunite-derived regolith and on 90 drill holes over pyroxenite-derived regolith (Fig. 1B). Samples were prepared to produce pulps finer than 150 mesh, followed by whole-rock analysis by X-ray fluorescence, producing results in weight % for: SiO_2, Al_2O_3, MgO, MnO, FeO, TiO_2, P_2O_5, CaO, Cr_2O_3, Ni, and Co (Putzolu *et al.* 2021). Analyses were performed at the SGS Geosol Laboratories Ltd in Belo Horizonte, Brazil. Concentrations below the detection limits are quoted as half of that value. The database also includes bulk dry density data of all regolith units (Tab. 1). These data were calculated by dividing the sample weight by its volume, obtained by immersion of sealed core samples in water and measurement of the displaced water volume.

Isocon and mass balance calculations

Mass balance has been applied in this work utilizing the isocon method (Grant 1986, 2005). The isocon analysis is aimed to assess the chemical mobility of elements and to quantitatively determine chemical gains and losses through mass transfer according to the Equation 1:

$$C_i^A = \frac{M^O}{M^A}(C_i^O + \Delta C_i) \quad (1)$$

Where:
C_i^A = the concentration of element (i) in the altered rock (A);
C_i^O = the concentration of element (i) in the original rock (O).
M^O and M^A = equivalent masses before and after alteration, respectively.
ΔC_i = the difference in concentration of the element between original and altered rock.

For each element or group of elements, there is an equation of this form in which M^O/M^A is constant. If immobile species are identified, for which $\Delta C_i = 0$, then M^O/M^A can be obtained by solving the set of simultaneous equations of the form (Eq. 2):

$$C_i^A = \frac{M^O}{M^A} C_i^O \quad (2)$$

The graphical representation is obtained by plotting the analytical data C_i^A against C_i, where the immobile (or least-mobile) elements that have been residually enriched define a straight line passing through the origin. The equation for this line, called an isocon, is calculated from its slope and it gives the overall changes in mass relative to M^O. Elements that fall below the line are leached, while those falling above are absolutely enriched (Fig. 3).

For the Santa Fé case, the isocon line was constructed from average geochemical results of all bedrock, saprock, green, ferruginous, and ochreous saprolite samples from all 535 drill holes over dunites. Samples above the ochreous saprolite were not used due to their transported colluvial nature, which could obliterate the original geochemical signature of the *in situ* profile. To determine the amount of rock required to develop the current regolith, the same methodology used by Golightly (2010), described in Velde and Meunier (2008), was applied. Starting from a concentration (C_i) of an immobile element (i) in a profile of a certain thickness (T) and a dry bulk

Table 1. Dry bulk density for each unit of the regolith profile.

Unit	Valid n	Dry bulk density (g/cm³)
Pisolitic soil	1,497	1.86
Iron crust	58	1.98
Trasition zone	421	1.52
Ochreous saprolite	146	1.13
Ferruginous saprolite	428	1.27
Green saprolite	1,319	1.38
Saprock	2,791	1.92
Serpentinized dunite	161	2.24

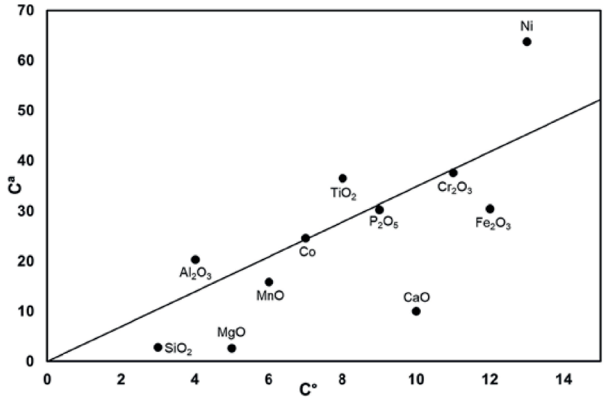

Figure 3. Isocon line constructed from an average geochemical result of 1893 samples originated from 535 drill holes over dunite saprolites (ochreous, ferruginous and green; Ca) and respective protolith (Co).

density (ρ), where "*o*" refers to the parent rock, the thickness of the parent rock (T^o) is given by Equation 3:

$$T^o = \frac{\Sigma(TC_i\rho)}{C_i^o \rho^o} \quad (3)$$

X-ray powder diffraction analysis

For the whole-rock XRPD analyses, six samples representing each regolith unit from pit SFPT-050S were split into approximately 200 g each and powdered in a disk mill, and in a McCrone Micronizing Mill to produce total sample portions of approximately 3 g. XRPD patterns were obtained with a Bruker-AXS D4 *Endeavour*, under the following operating conditions: Ni Kβ-filtered CoKα radiation from a sealed tube operated at 40 kV and 40 mA, measured from 4 to 105° 2θ at 0.02° step and 1 s/step with a LynxEye position-sensitive detector. Mineral interpretation was performed using the Bruker-AXS's Diffrac.EVA 5.0 software and the PDF04+ database (International Center for Diffraction Data – ICDD). The mineral quantification was conducted by the full Rietveld method refinement, using fundamental parameters (Cheary and Coelho 1992), on software DIFFRAC.TOPAS 5 or 6 (Bruker-AXS). The background was modeled by 6th order polynomial, and the five CuKα emission lines of Berger (1986) with an additional Kβ line by Hölzer *et al.* (1997) were fitted, the latter one refined to account for minor Kβ not eliminated by the filter. Other fitted instrumental parameters were sample displacement and absorption. The refinement does not take into account the presence of amorphous matter, as no amorphous-related bulge from 15 to 40° 2θ has been observed.

Additionally, the fine-grained fraction (< 2 μm) of the same four samples from pit SFPT-050S (*i.e.* saprock, green and ferruginous saprolites) were analyzed to identify the clay mineralogy. The clay fraction was obtained by standard techniques including sieving, centrifuging, and pipetting, also described in Putzolu *et al.* (2020). They were subsequently treated to eliminate all free iron. Thus, the preferred oriented samples were then analyzed to produce air-dried, solvated by ethylene glycol, and heat at 550°C XRPD diffractograms. The interpretation of the diffractograms was carried out based on Santos (1975), Thorez (1975), and Dixon (1989).

Scanning electron microscopy with energy dispersive spectroscopy and electron microprobe analysis

Scanning electron microscopy with energy dispersive spectroscopy (SEM-EDS) and electron microprobe analysis (EMPA) analyses were performed on 11 core samples from drill holes SFDD-017 (3), SFDD-041 (1), SFDD-308 (3), and FDSF-01 (4) (Fig. 1B) that best represent the regolith units over the serpentinized dunite. SEM-EDS analysis was carried out on polished thin sections using a ZEISS EVO LS 15 scanning electron microscope at the Natural History Museum (NHM, London) operating at 20 kV, and current of 3 nA. For field emission SEM, high-resolution elemental maps were carried out by a FEI Quanta 650 FEG SEM mounting Bruker Flat Quad 5060F energy dispersive X-ray fluorescence spectroscopy detectors (EDS) for hyperspectral mapping. The energy-dispersive X-ray (EDX) maps were acquired through high vacuum (HV) mode and the instrument operated at 15 kV, with 28 mm working distance and a pixel size of 8 μm. For EMPA, quantitative data sets were obtained by wavelength dispersion spectrometry (WDS), at the NHM, using a Cameca SX100 electron microprobe operating at 20 kV, 20 nA, and 10 μm in spot size. EMPA data was also obtained at Universidade Federal do Rio de Janeiro (UFRJ), with the Jeol JXA-8230 instrument equipped with a 5 Wavelength Dispersive Spectrometer (WDS), using the same operating parameters of the NHM.

The structural formulas of chlorite and serpentine were calculated on the basis of 14 oxygens, and serpentine on the basis of 7 oxygens. Iron was considered to be present as Fe^{+2}.

RESULTS

Geochemistry of the lateritic profile

The whole-rock geochemical data of the core samples from all regolith units and protolith were extensively studied by Putzolu *et al.* (2021) using multivariate statistical analyses, *i.e.*, principal component analysis and factor analysis. In this

work, prior to the mass balance study, box and whisker plots were used to describe the geochemical distribution of the elements in the laterite units.

Results for Ni are shown in the box and whiskers plots in Figure 4A. It confirms that the ferruginous and ochreous saprolites are the main Ni bearing units with median Ni grades of 1.50 and 1.44 wt%, respectively. In the green saprolite and saprock, Ni grades are lower (0.68 and 0.22 wt% Ni, respectively), although outliers high-grade intervals occur likely reflecting mineralization in open spaces in fractures close to the weathering front (Golightly 2010). There is a clear Ni depletion trend from the transition zone upward into the iron crust and

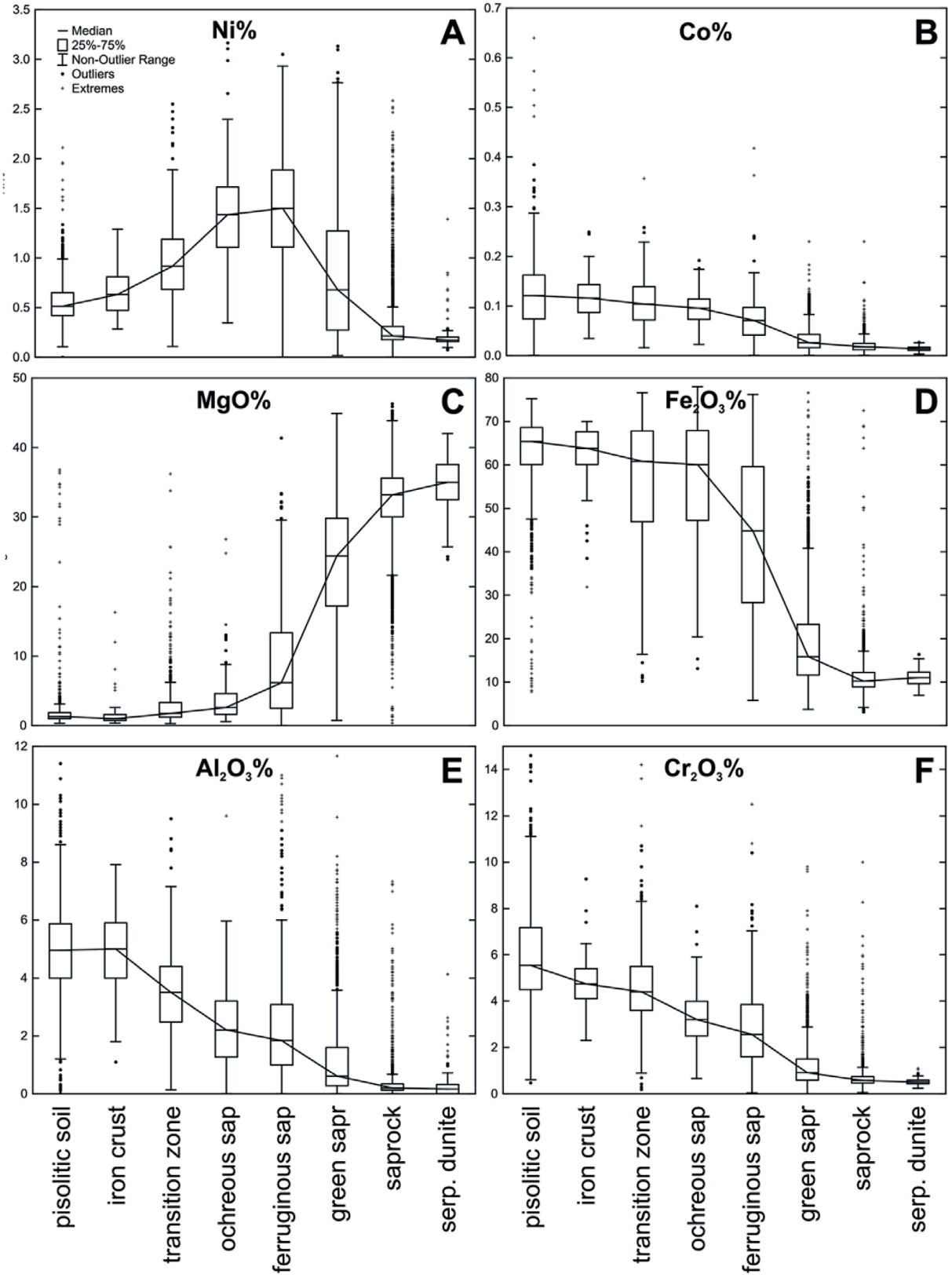

Figure 4. Box and whisker plots of whole-rock major oxides of the deposit unit subtypes.

pisolitic soil. Cobalt is concentrated in the ferruginous zones with a median grade close to 0.1 wt% (Fig. 4B). Silica and Mg (Fig. 4C) are strongly leached upward and this is accompanied by increasing ferruginization of the regolith (Fig. 4D). Aluminium (Fig. 4E) is also enriched upward.

Isocon and mass balance

Determining immobile elements for mass balance calculations is a difficult task, but if the ratio of element concentrations in the regolith over protolith are compared in all saprolite units, it suggests that Cr is relatively immobile. In the isocon plot (Fig. 3), it is possible to observe that the best-fitting isocon line can be drawn through Cr and Co, which is persistent in all saprolite units, even if Figure 3 represents just an average overview of the saprolite. This is consistent with the findings of Putzolu *et al.* (2021), who demonstrated that a fraction of Co occurs in association with Cr- and Fe-spinels chromite, and such deportment in the deposit is not altered by the supergene process. A unit-by-unit analysis focusing on Al-Ti immobility did not define an isocon line with the characteristics of immobile elements, as described by Grant (2005).

Through the analyses of the isocon line, Cr and Co could be considered the least-mobile elements, but the mass balance calculation was applied using only Cr as the reference element, due to trace amounts of Co. Chromium shows a progressive enrichment trend upward in the regolith (Fig. 4F). Outlier values for Cr were identified and disregarded in order to obtain the average value of C_i^A and C_i^O (Eq. 2).

The results of the mass balance in terms of mass change of elements in the profile over pyroxenites and dunites are plotted in Figure 5. They show that Ni is depleted from the transition zone upward and enriched in the saprolite units (Fig. 5A). Mobile elements, *i.e.* Mg and Si, are clearly leached across the whole regolith profile. In this frame, less mobile elements such as Fe are also weakly leached from the saprolite upward (Fig. 5A). Although these latter elements appear depleted compared to Cr, their total concentration rises upward in the profile (Fig. 4), as their residual enrichment is preponderant over their depletion by leaching. The geochemical trends observed for these metals, with the notable exception of Co (Putzolu *et al.* 2021), are consistent with their general behavior in Ni lateritic profiles (Golightly 1981, Schellmann 1983, Nahon and Tardy, 1992, Elias 2002, Gleeson *et al.* 2003, Al-Khirbash 2015, Putzolu *et al.* 2019).

Al and Ti show a clear enrichment trend in the regolith over the dunite (Fig. 5C), especially in the green and ferruginous saprolites where Ni and chlorites are also most abundant, indicating that these elements, along with Ni, have been absolutely enriched in the current profile. On the other hand, over the pyroxenites, Al and Ti are residually enriched in

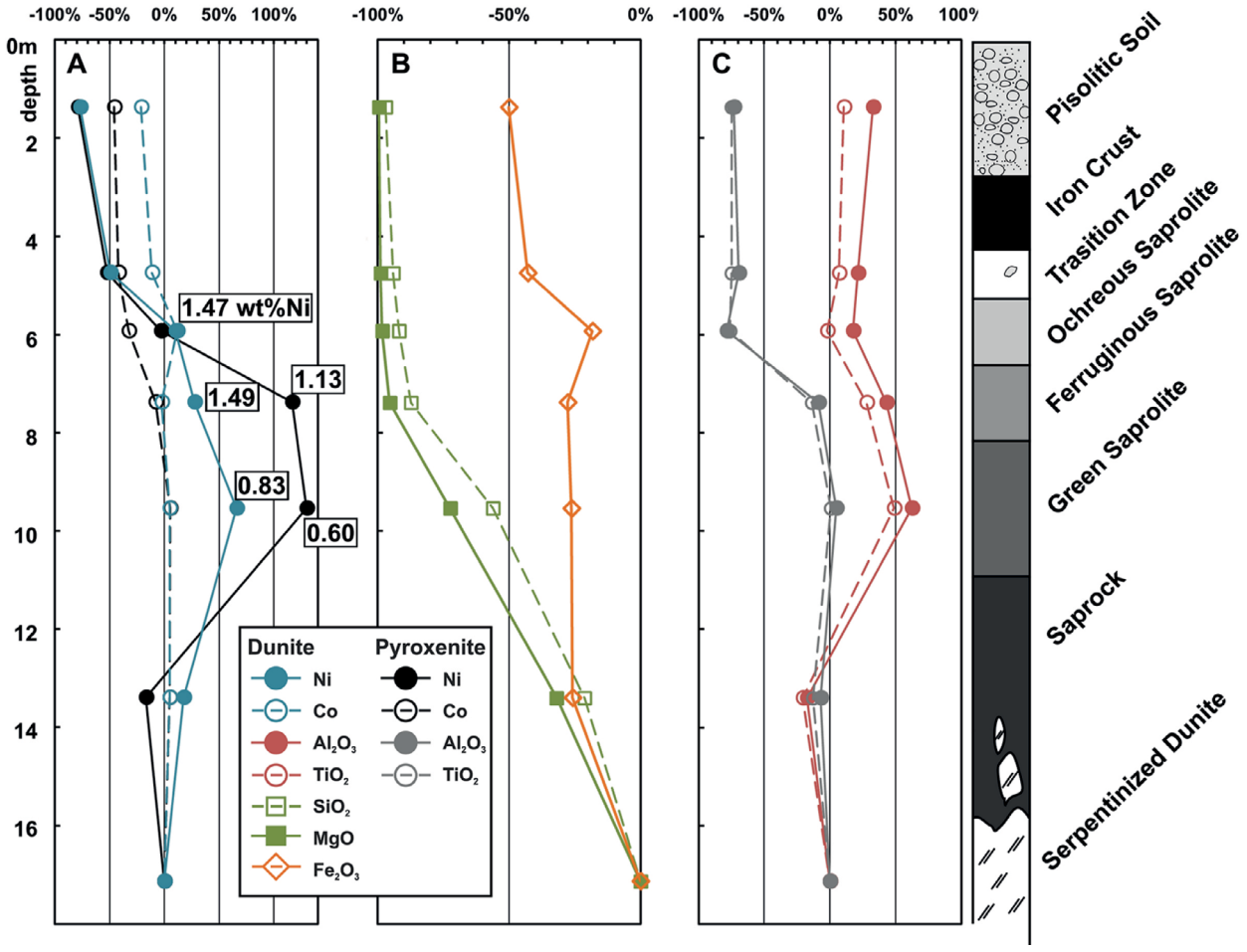

Figure 5. X axis: Elements gains and losses percentages relative to each parent-rock along with the profile, based on Cr immobility.

the saprock, green and ferruginous saprolites, but are actually leached from the ochreous saprolite upward (Fig. 5C).

To determine the thickness of protolith required to develop the current lateritic profile (Eq. 3), Cr was used as the reference element and the average bulk dry density for each horizon and protolith are shown in Table 1. The result shows that about 46 m of protolith have been consumed in order to produce the present-day regolith, having an average thickness of 11.4 m. Alternatively, if Al or Ti were considered as reference elements, the results would be 61.9 and 49.6 m, respectively. The latter are probably overestimations, given that the silcrete hilltops lie at approximately 50 m above the present surface (Golightly 2010), which would imply that there was practically no mass loss during *Velhas* surface evolution, which is quite unlikely. With mass balance calculations (Eq. 3), it has also been possible to show that a total of 27.2 m of dunite bedrock was necessary to supply the present abundance of Ni in the current profile.

Mineralogy XRPD

Oliveira and Trescases (1980), Carvalho e Silva and Oliveira (1995), Putzolu *et al.* (2021) presented an extensive mineralogical study of the Santa Fé profile. In the present work, the clay mineralogy has been further characterized by XRPD analysis in the fine-grained fraction, and the mineralogical assemblage was further investigated by quantitative XRPD (Rietveld method). The XRPD results of the clay fraction from saprock and saprolite showed clay species of the chlorite and serpentine groups.

The results of the Rietveld analyses are shown in Table 2 and Figure 6, while the XRPD patterns of samples from the

Table 2. Quantification of minerals after Rietveld refinement, followed by the weighted profile R-factor and the goodness of fit for each refinement.

SFPT-050S	Upper pisolitic soil	Lower pisolitic soil	Ochreous saprolite	Ferruginous saprolite	Green saprolite	Saprock
Chromite	14.4	11.7	9.6	8.3	3.6	2.3
Chlorite	-	-	**9.4**	**17.5**	**14.0**	**8.1**
Gibbsite	1.4	1.9	-	-	-	-
Goethite	1.6	12.7	27.7	26.3	20.3	16.8
Hematite	42.8	50.6	35.3	18.7	-	-
Lizardite	-	-	-	3.7	38.6	63.7
Magnetite	30.2	17.4	14.5	22.2	8.2	4.4
Quartz	9.6	5.5	3.6	3.4	13.3	4.7
Vermiculite	-	-	-	-	2.0	0.03
Total	100.0	100.0	100.0	100.0	100.0	100.0
Rwp	2.2	2.2	2.4	2.5	3.2	3.5
GOF (X)	1.9	1.8	2.1	2.1	5.0	5.8

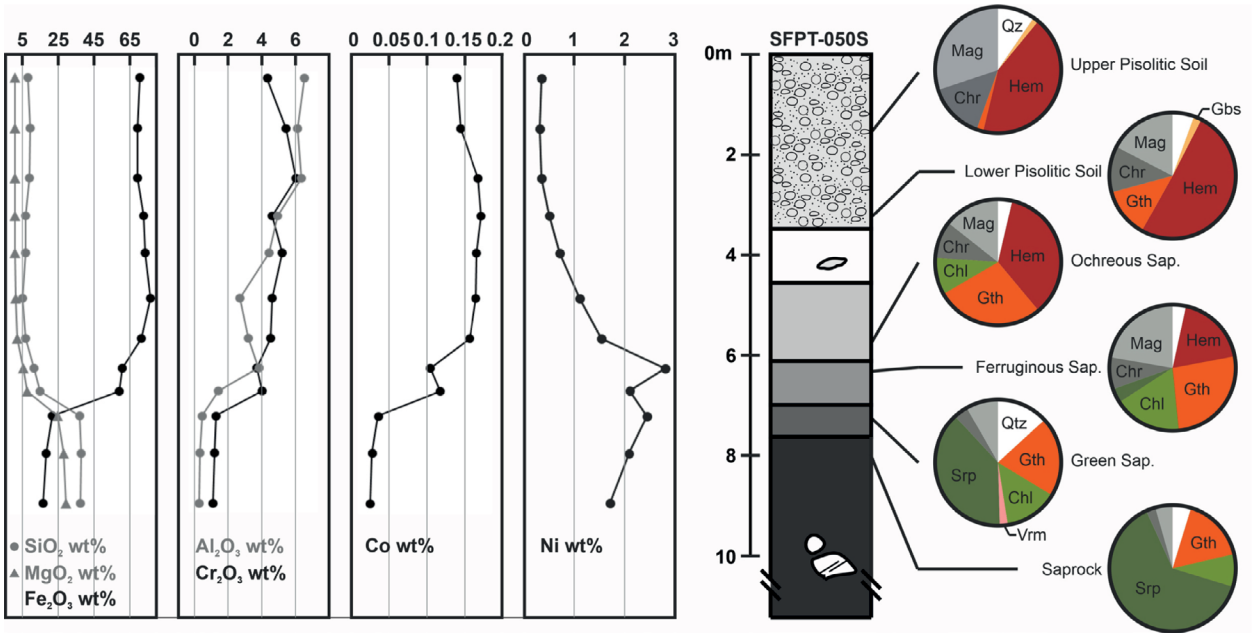

Figure 6. Geochemical logs along with the pit SFPT-050S and Rietveld Quantification analysis.

pisolitic soil, ferruginous and green saprolites are shown in Figure 7 and Table 3.

The saprock is dominated by serpentine (63.7 wt%), with lower amounts of goethite and chlorite (16.7 and 8.7 wt%, respectively). Spinel-group minerals (*i.e.* magnetite and chromite) have been recorded in significant amounts in the saprock varying from 2 to 4%. Putzolu *et al.* (2021) recognized two types of serpentine based on their textures and Ni contents. Serpentine I has a massive and mesh-like texture, is primary and Ni-poor (Fig. 8A). Serpentine II occurs as micro vein fillings and is Ni-rich.

In the green saprolite, the serpentine amount decreases to 38.6 wt%, while chlorite becomes an important component with 14 wt%. Oliveira and Trescases (1980) and Putzolu *et al.* (2021) describe the occurrence of primary chlorites around chromites (Fig. 8B). However, in the present work it has been also observed that chlorite is also disseminated in the matrix (Figs. 8C and 8D). Goethite occurs in significant amounts (20.3 wt%), mostly disseminated in a fine-grained matrix (Figs. 8C-8F). The amount of residual resistate grains, such as chromite and magnetite, is also

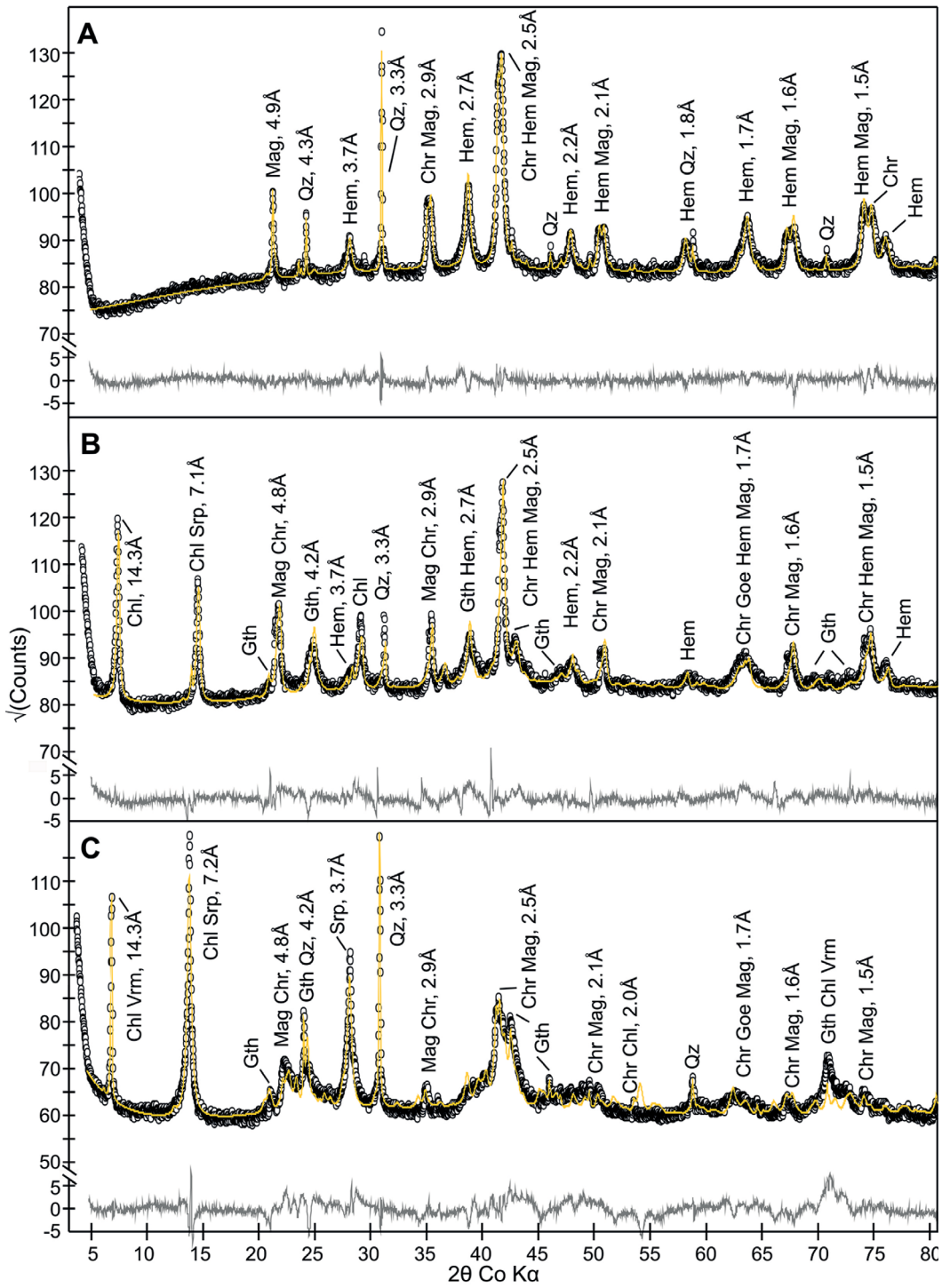

Chl: chlorite; Chr: chromite; Gbs: Gibbsite; Gth: goethite; Hem: hematite; Mag: magnetite; Qz: quartz; Srp: serpentine; Vrm: vermiculite.

Figure 7. XRPD pattern of the bulk rock. Circles represent points' counts; yellow line represents Rietveld refinement model; the grey line shows the error values, and represents the difference between the collected points and the adjustment curve; (A) upper pisolitic soil; (B) ferruginous saprolite; (C) green saprolite.

Table 3. Chemical composition of selected chlorites and serpentines.

	chlorite												serpentine					
Oxides	**ochreous saprolite**			**ferruginous saprolite**			**green saprolite**			**saprock**			**I**			**II**		
SiO_2	39.4	35.3	29.5	34.3	34.3	29.7	42.8	39.96	31.7	37.5	34.7	36.3	41.8	36.4	36.7	35.6	39.9	38.9
FeO	3.6	6.6	11.1	4.3	6.8	5.2	2.9	3.08	9.4	5.1	5.6	11.0	6.4	7.7	6.8	7.0	9.2	6.2
MgO	23.7	21.8	19.9	22.1	22.9	20.1	25.6	26.29	16.8	23.3	24.1	24.8	37.1	31.7	32.7	29.7	34.0	34.0
Al_2O_3	12.0	9.7	9.7	12.5	9.3	14.6	12.2	10.90	6.8	12.5	13.1	2.2	0.9	0.0	0.1	0.9	0.6	0.0
TiO_2	1.6	0.7	0.8	3.8	0.6	1.7	1.9	2.06	2.7	5.0	4.6	0.1	0.1	0.0	0.0	0.1	0.1	0.0
Cr_2O_3	0.40	0.23	0.15	0.94	0.19	0.13	0.36	0.39	0.03	0.99	1.20	0.07	0.03	0.06	0.15	0.12	0.10	0.00
MnO	0.12	0.07	0.00	0.00	0.09	0.08	0.00	0.00	0.08	0.06	0.05	0.04	0.04	0.01	0.03	0.04	0.12	0.21
CoO	0.00	0.52	0.04	0.00	0.00	0.10	0.22	0.13	0.01	0.11	0.00	0.14	0.01	0.09	0.00	0.01	0.00	0.01
NiO	4.5	9.7	6.5	2.0	5.1	10.4	1.2	1.40	2.6	1.0	1.4	6.4	1.1	0.2	0.4	1.6	1.3	2.6
Total	85.3	84.7	77.6	79.9	79.3	82.1	87.1	84.2	70.1	85.6	84.7	80.9	87.4	76.2	76.9	75.0	85.3	81.8
APFU																		
Si	3.81	3.65	3.40	3.54	3.69	3.17	3.94	3.84	3.87	3.60	3.41	3.97	1.99	2.01	2.00	2.00	1.99	2.00
Al_{IV}	0.19	0.35	0.60	0.46	0.31	0.83	0.06	0.16	0.13	0.40	0.59	0.03	0.01	0.00	0.00	0.00	0.01	0.00
Σ_{tet}	4.00	4.00	4.00	4.00	4.00	4.00	4.00	4.00	4.00	4.00	4.00	4.00	2.00	2.01	2.00	2.00	2.00	2.00
Fe	0.29	0.57	1.07	0.37	0.61	0.47	0.22	0.25	0.96	0.41	0.46	1.00	0.26	0.35	0.31	0.33	0.38	0.27
Mg	3.42	3.36	3.41	3.40	3.67	3.21	3.51	3.76	3.06	3.34	3.53	4.04	2.63	2.61	2.66	2.49	2.52	2.61
Al_{VI}	1.17	0.83	0.71	1.06	0.87	1.02	1.26	1.07	0.85	1.02	0.92	0.25	0.04	0.00	0.00	0.06	0.02	0.00
Ti	0.11	0.06	0.07	0.30	0.05	0.14	0.13	0.15	0.25	0.36	0.34	0.01	0.00	0.00	0.00	0.00	0.00	0.00
Cr	0.03	0.02	0.01	0.08	0.02	0.01	0.03	0.03	0.00	0.08	0.09	0.01	0.00	0.00	0.01	0.01	0.00	0.00
Mn	0.01	0.01	0.00	0.00	0.01	0.01	0.00	0.00	0.01	0.01	0.00	0.00	0.00	0.00	0.00	0.00	0.00	0.01
Co	0.00	0.04	0.00	0.00	0.00	0.01	0.02	0.01	0.00	0.01	0.00	0.01	0.00	0.00	0.00	0.00	0.00	0.00
Ni	0.35	0.81	0.60	0.16	0.44	0.90	0.09	0.11	0.26	0.07	0.11	0.56	0.04	0.01	0.02	0.07	0.05	0.11
Σ_{oct}	5.38	5.70	5.87	5.37	5.66	5.76	5.26	5.38	5.39	5.29	5.45	5.88	2.98	2.98	3.00	2.96	2.99	3.00
Structural formulae calculated on the basis of										$O_{10}(OH)_8$						$O_5(OH)_4$		

relevant (3.6 and 8.2 wt%, respectively). Vermiculite was detected, during XRPD and Rietveld refinement interpretation, both in the saprock and in the green saprolite, in amounts up to 2 wt%, but it has not been observed as part of the saprolite matrix.

In the ferruginous saprolite, hematite and goethite are the main minerals with amounts of 18.7 and 26.2 wt%, respectively. Chlorite is also abundant (17.5 wt%), while the serpentine amount is subordinate (3.6 wt%). Magnetite and chromite are further enriched to 22.2 and 8.3 wt% respectively.

The ochreous saprolite is richer in Fe-oxides and Fe-hydroxides, such as hematite (35 wt%) and goethite (27.7 wt%) (Fig. 8E). The amount of spinel-group minerals (magnetite and chromite) is also high (24.1 wt%), but chlorite decreases to 9.4 wt%. The reduction of serpentine and chlorite is correlated with the relevant drop in the bulk amount of SiO_2 and MgO observed at the border between the green saprolite and the ferruginous saprolite (Fig. 4C). This is a peculiar geochemical trend, *i.e.*, the well-known Mg-discontinuity, which is globally recognized in Ni-laterite ores (*e.g.* Butt and Cluzel 2013, Putzolu *et al.* 2019).

In pisolitic soil, magnetite and chromite become increasingly concentrated from the lower to the upper portion (Fig. 8E). Chromite concentration increases from 11.7 to 14.4 wt% and magnetite increases from 17.4 to 30.2 wt%. In this unit, Fe-oxy-hydroxides are dominated by hematite (50.6 to 42.8 wt%), with minor goethite (12.7 to 1.57 wt%).

The XRPD goethite peaks show a high full width at half maximum (FWHM), which reflects the small crystallite size of goethite.

Quartz is detected as a minor component and is probably derived from scattered silcrete fragments throughout the profile, as well as from the serpentinization process of olivine (Putzolu *et al.* 2021).

Mineral chemistry: SEM, EMPA, and high-resolution elemental maps

SEM and EMPA analyses of representative samples were conducted to evaluate the composition of: serpentine type I and II; chlorites from saprock, green saprolite, ferruginous saprolite, and ochreous saprolite; Fe-oxy-hydroxide in the matrix of the green saprolite, ochreous saprolite, and pisolitic soil; Fe-oxy-hydroxide forming core and rims of pisolites; Fe-oxy-hydroxide pseudomorphs after Fe-Mg minerals from all saprolite units. Results are displayed in the box and whisker plots of Figure 9.

Mn-oxy-hydroxides, which were extensively studied by Putzolu *et al.* (2021), were also observed in small veinlets or

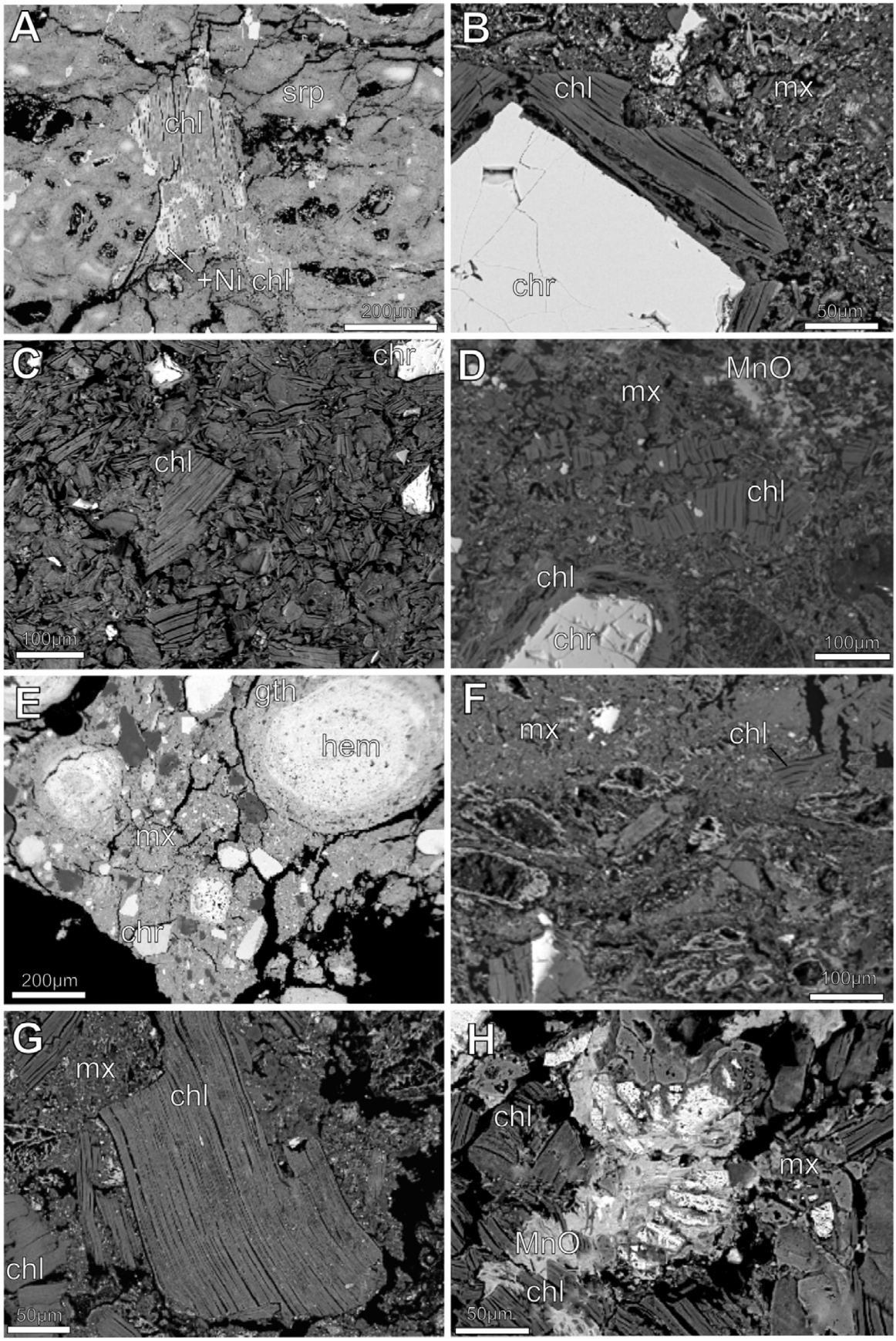

Chl: chlorite; srp: serpentine; gth: goethite; chr: chromite; hem: hematite; mx: Fe matrix.

Figure 8. Backscattered electron photomicrographs showing the typical textures of the newly formed phyllosilicates and oxides. (A) chlorite in mesh serpentine texture (saprock); (B) hydrothermal chlorite paragenesis with a Cr-spinel grain in goethite matrix (ochreous saprolite); (C) disseminated chlorite, goethite typical texture of ferruginous saprolite; (D) Cr-spinel chlorite association with detrital matrix chlorite and Mnoxide agglomerate (ferruginous saprolite); (E) goethite/hematite pisolites in goethitic matrix, with residual spinels in non-cohesive material (pisolitic soil); (F) olivine Fe-oxide pseudomorphs on lower half zone and goethite matrix with detrital chlorite on the upper half (saprock); (G) goethite matrix with detrital chlorite (ochreous saprolite); (H) porous matrix with chlorite predominance and agglomerates of Mn-Fe-oxide (green saprolite).

agglomerations (Fig. 8H). Although Mn-oxy-hydroxides occur in much smaller amounts, they show the highest Ni (med = 16 wt% NiO). Pisolites and oolites show invariably low Ni grades. The impact of these phases on the distribution of Ni and Co was thoroughly discussed in Putzolu *et al.* (2021) and therefore will not be further addressed here.

The Ni content of chlorite increases upward from the saprock (1.6 wt% NiO) to ochreous saprolite (7.2 wt% NiO). The Ni content of serpentines I is 0.5 wt% NiO, while in serpentine II it is 1.7 wt% NiO, with a higher variance than serpentine I, reaching up to 3.9 wt% NiO.

The median Ni grades of the Fe-oxy-hydroxides in the matrix of the green saprolite and the ochreous saprolites is about 2.0 wt% NiO, but drop drastically in the ferruginous matrix of the pisolitic soil (0.6 wt% NiO) following the strong tendency of Ni depletion observed through whole-rock geochemical analysis.

Serpentine

The microprobe data confirm the occurrence of two types of serpentine, which can be classified based on their Ni grades. Examples of their composition are given in Table 3, while their average mineral formulas are the following:

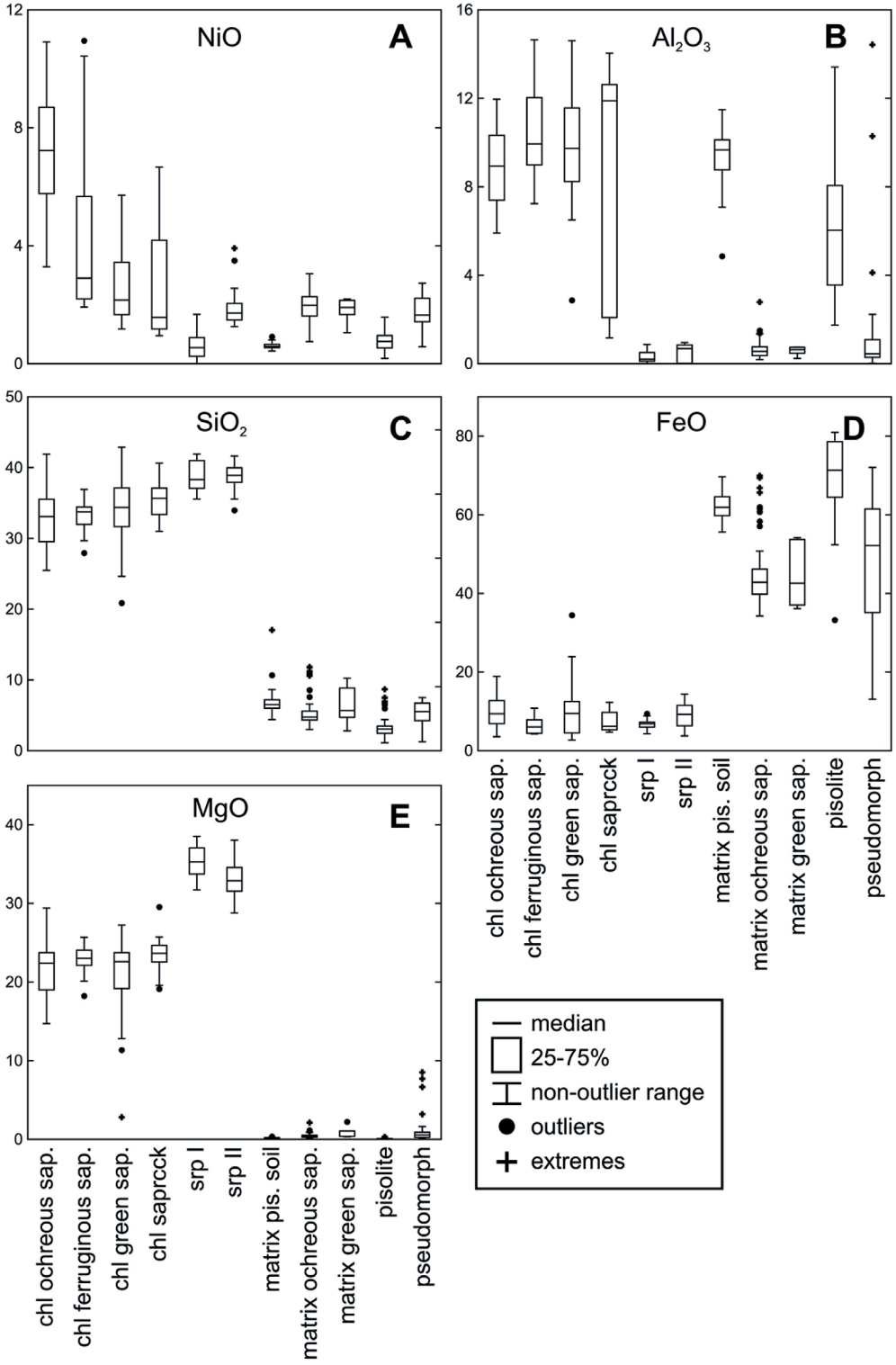

Figure 9. Box and whisker plots of EMPA analysis grouped by mineral, material and subtypes.

$$srp\ I\ (Mg_{2.69}Fe^{2+}_{0.28}Ni_{0.02}Al_{0.01})_{3.00}(Si_{1.98}Al_{0.01})_{1.99}O_5(OH)_4$$
$$srp\ II\ (Mg_{2.50}Fe^{2+}_{0.39}Ni_{0.08}Al_{0.01})_{2.98}(Si_{1.98}Al_{0.02})_{2.00}O_5(OH)_4$$

Magnesium is the major cation of the octahedral site and shows a strong negative correlation with Ni, suggesting that Ni is replacing Mg (Fig. 10).

In the Mg-Si-(Fe-Ni) diagram, the serpentines from Santa Fé fall in the lizardite field (Fig. 11). They show a similar composition to the Ni serpentines from Niquelândia, Wingellina, Cerro Matoso, and Soroako deposits and show a slight chemical fluctuation following the solid solution between the Ni+Fe and Mg end members. However, serpentine I has higher median Ni grade compared to Niquelândia, Cerro Matoso, and Wingellina (Colin *et al.* 1990, Gleeson *et al.* 2004, Putzolu *et al.* 2020).

The Ni content of serpentine II is higher than in Wingellina, although some analyses from the latter deposit show a significant enrichment following the serpentine series solid solution line (Fig. 11). In this frame, serpentine from Soroako has higher Ni content than those occurring in Santa Fé. However, in Santa Fé, few outlier analyses reach high grades.

The serpentines from Santa Fé have a lower total Al amount among all compared deposits, with Al having a positive correlation with Ni content (Fig. 12). Overall, the Al gain of serpentine II is greater than on serpentine I, except for a group of samples of serpentine II where Al amount is lower, yet still having high Ni content.

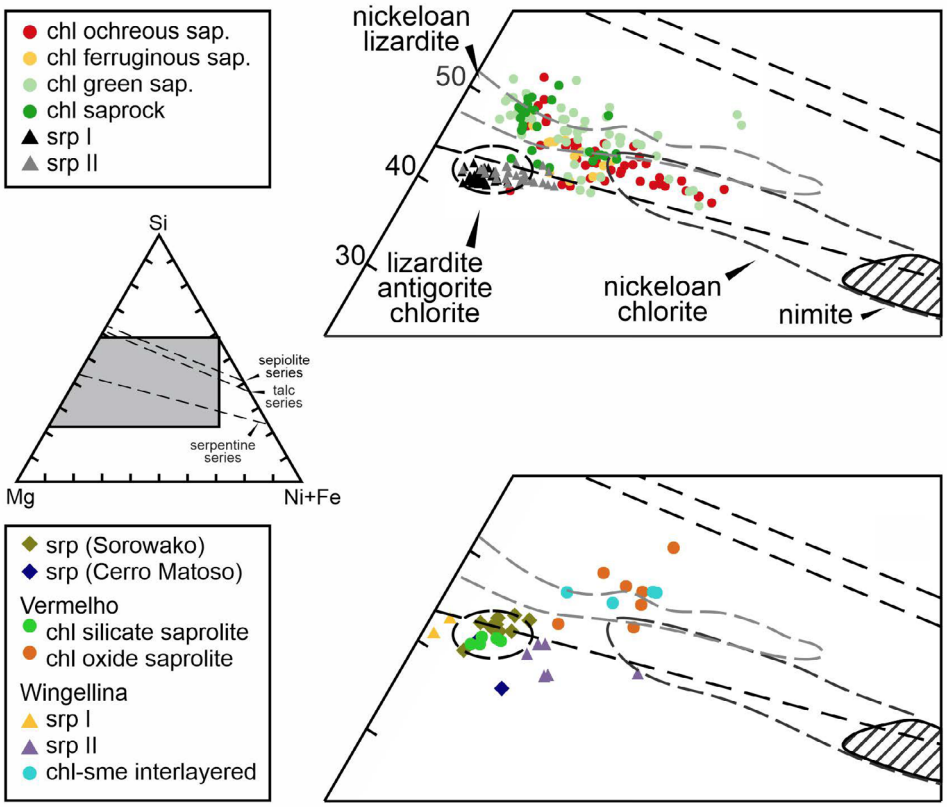

Figure 11. Si:Mg:(Fe+Ni) ratios for crystalline Ni-bearing hydrous silicates (Brand *et al.* 1998). Data from Sorowako, Vermelho, Cerro Matoso, and Wingellina respectively from Golightly and Arancibia (1979), Carvalho e Silva (1994), Gleeson *et al.* (2004), Putzolu *et al.*(2020).

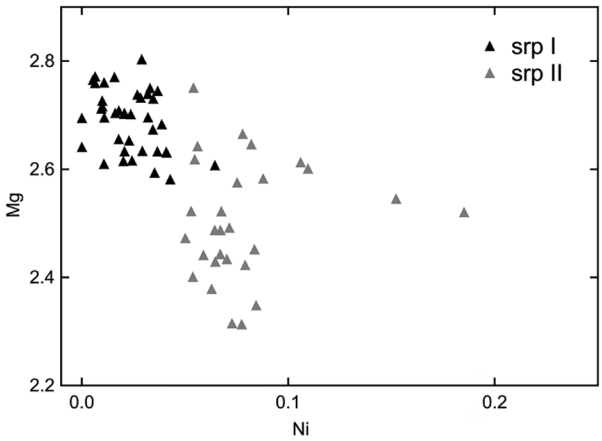

Figure 10. Ni:Mg scatter plot for serpentines. Variables are expressed in apfu.

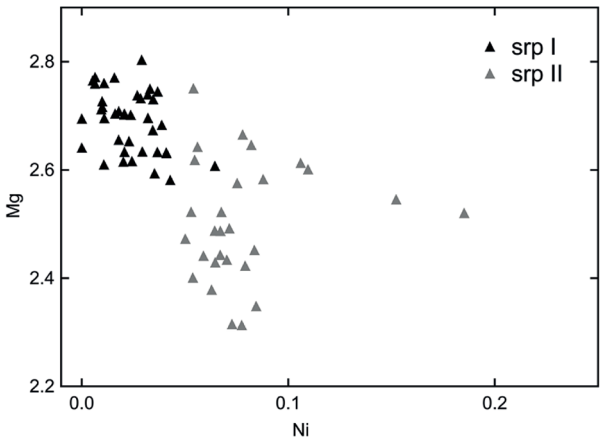

Figure 12. Ni:Total Al scatter plot for serpentines. Variables are expressed in apfu.

Chlorite

Representative EMPA analyses are given in Table 3, while their average mineral formulas are the following:

Ochreous Saprolite
$(Al_{0.67}Mg_{3.48}Fe^{2+}_{0.92}Ni_{0.62})_{5.69}(Si_{3.54}Al_{0.46})_{4.00}O_{10}(OH)_8$;
Ferruginous Saprolite
$(Al_{0.87}Mg_{3.65}Fe^{2+}_{0.59}Ni_{0.38})_{5.49}(Si_{3.56}Al_{0.44})_{4.00}O_{10}(OH)_8$;
Green Saprolite
$(Al_{0.87}Mg_{3.36}Fe^{2+}_{0.95}Ni_{0.23})_{5.41}(Si_{3.64}Al_{0.36})_{4.00}O_{10}(OH)_8$;
Saprock
$(Al_{0.73}Mg_{3.63}Fe^{2+}_{0.65}Ni_{0.24})_{5.25}(Si_{3.68}Al_{0.32})_{4.00}O_{10}(OH)_8$.

The main octahedral cation is Mg, which varies slightly among chlorite from the different saprolites. Another major component of the octahedral sheet is Fe^{2+} with median contents varying from ~5 to 9.5wt% FeO in the saprolite units. Chlorites from the ochreous saprolite (med = 7.2 wt% NiO) are nearly two to three times richer in Ni than those of the ferruginous saprolite (med = 2.9 wt% NiO), green saprolite (med = 2.2 wt% NiO), and saprock (med = 1.6 wt% NiO).

Chlorites from the ferruginous and ochreous saprolite show lower Si contents compared to those from green saprolite and saprock. The amount of Al reaches the lowest values in the ochreous saprolite (med = 8.9 wt% Al_2O_3). However, although the Al median value in the saprock is the highest (med = 11.9 wt% Al_2O_3), there is a group of samples that are depleted in Al if compared to the saprolite (Fig. 9B). The tetrahedral charge imbalance is compensated by the introduction of trivalent cations in the octahedral sheet, mostly Al. Therefore, the best fit for Mg substitution is the one depicted in Figure 13A, where the main substituting cations are Fe^{2+}, Ni, Al^{VI}, and Ti. Moreover, a moderate positive correlation between Ni and Fe was also observed in the diagram in Figure 13B, which represents the substitution proportion of Ni and Fe for Mg cations on octahedral sites. In green saprolite and saprock, the Fe^{2+}/Ni ratio is higher than in the ferruginous and ochreous saprolites.

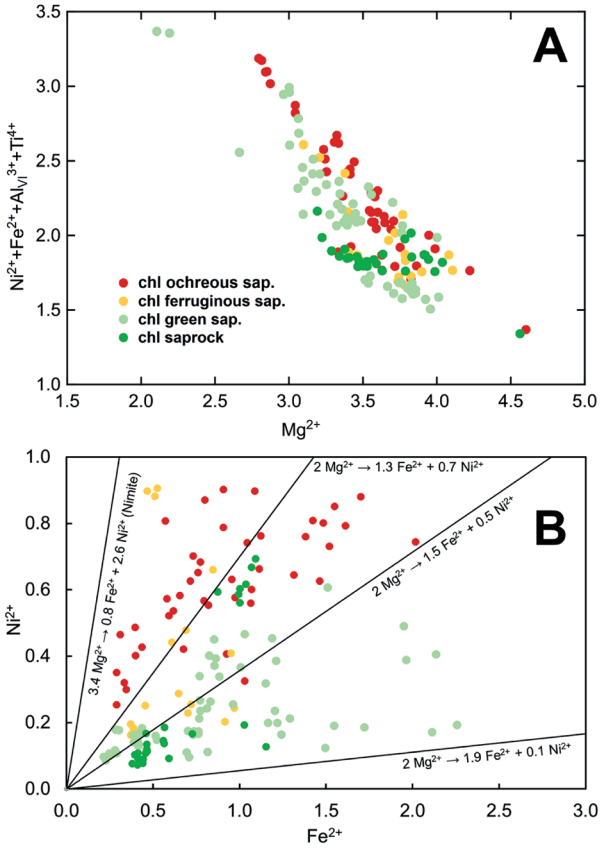

Figure 13. Binary plots showing the mineral chemistry of chlorites. Variables are expressed in apfu.

The EDX maps (Figs. 14A and 14B) confirm that chlorites host high Al and Ni contents, with the Ni-rich areas coincident with Fe-rich and Al-Mg-poor areas (Fig. 14A). As shown by Figure 11, chlorite from Santa Fé, although Ni- and Fe-rich, cannot be classified as nimites (Ni-chlorite) or chamosites (Fe-chlorite), but can be defined as nickeliferous clinochlore (Foster 1962, Wiewióra and Weiss 1990, Brand *et al.* 1998).

Figure 11 shows that the enrichment of Ni+Fe in the chlorites from the ferruginous and ochreous saprolites is accompanied by Mg and Si depletion following an increasing leaching, as has also been observed in the Vermelho deposit (Bernardelli *et al.* 1983, Carvalho e Silva and Oliveira 1995). In some chlorites from saprock the Ni+Fe relative concentrations are distinctly higher, giving rise to a separate cluster, more similar to those from green and ferruginous saprolite.

Iron oxy-hydroxides

EMPA analyses conducted on the whole textural elements are reported in Table 4. The matrix of the pisolitic soil is the richest in Fe (61.9 wt% FeO_t, Fig. 9), while in the ochreous and green saprolite the Fe content is of approximately 43 wt%, suggesting a variable degree hydration and variable proportion between the hematitic and goethitic components.

The Ni content in Fe-oxy-hydroxides of the ochreous saprolite is correlated with the Al content (Fig. 15A), with the latter that in turn has a well-fitting relationship with Mg and Ti (Figs. 15B and 15C). These chemical trends could suggest the occurrence of sub-microscopic disseminations of fine-grained chlorite in the matrix (Figs. 8B, 8D and 8G).

The rims of pisolitic Fe-oxy-hydroxides are characterized by higher Al content, and thus by lower Fe when compared to the core (Fig. 15D). It has also been observed that Ni is slightly more enriched at the rim (Fig. 15D), and that the Ni concentrations in the goethite cortex (0.97 wt% NiO) are higher than in the hematite core (0.80 wt% NiO) of the pisolites.

The geochemical properties of Fe phases can be interpreted using the triangular plot of Figure 16. The Ni enrichment in the ferruginous matrix of the ochreous saprolite is associated with a slight Al enrichment. Ni-Al joint concentration is not observed in the ferruginous pseudomorphs, where Ni is gained as a function of the alteration of the Al-poor skeletal olivine grains. In the ferruginous matrix of the pisolitic soil Ni grades are at levels similar to those of cores and rims. The main chemical variation occurs along the Fe-Al substitution line, which is partly associated with a slight Ni enrichment at the rims.

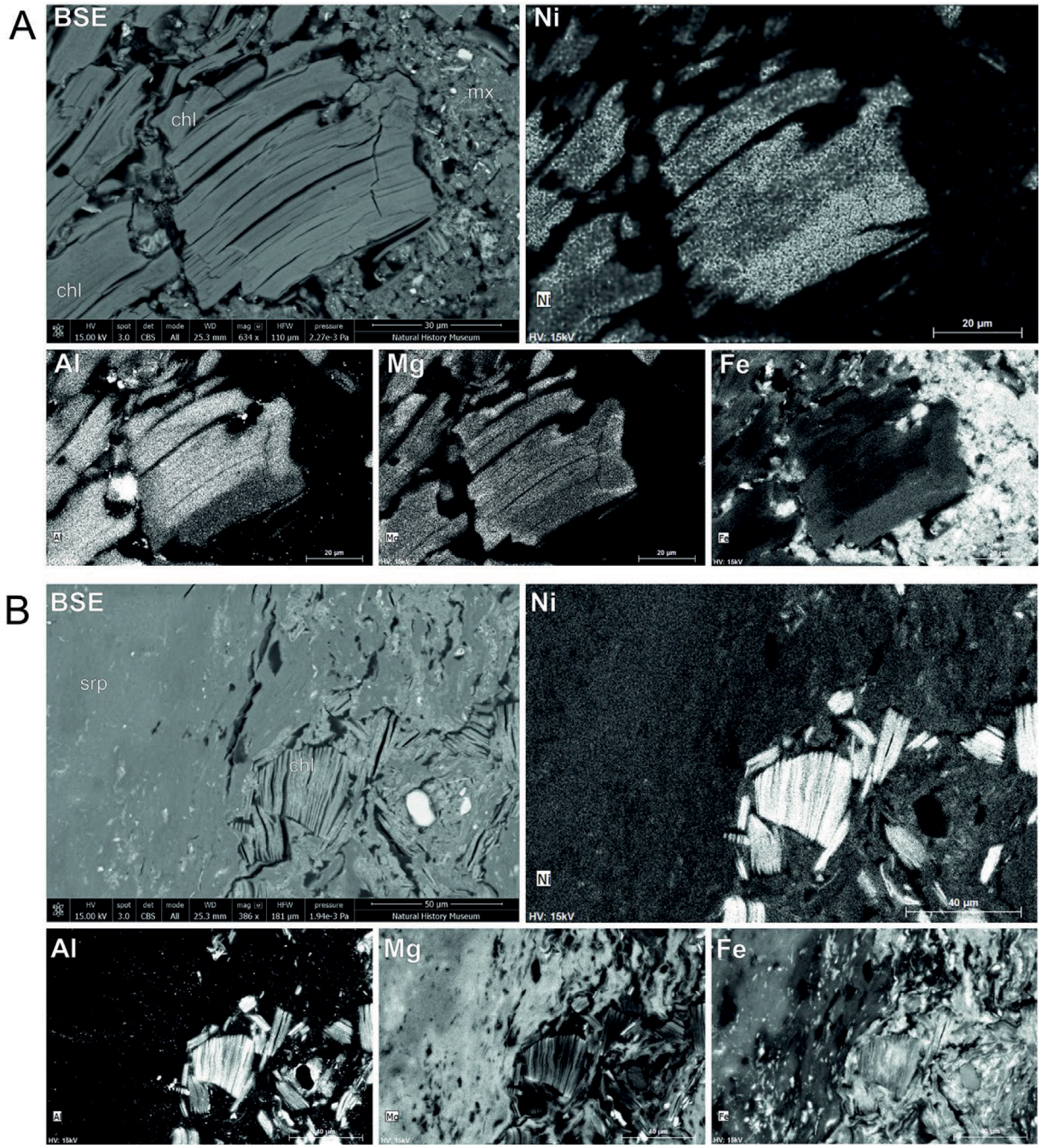

Figure 14. EDX high-resolution maps: (A) chlorite surrounded by a ferruginous matrix; (B) ochreous saprolite-like / green saprolite-like interface.

Table 4. Chemical composition of selected Fe-oxy-hydroxides.

	goetitic matrix pisolitic soil			pisolith rim			pisolith core			goetitic matrix ochreous saprolite			goetitic matrix green saprolite			olivine Fe oxide pseudomorph		
SiO_2	5.8	6.6	10.7	2.8	6.7	3.9	1.3	1.9	3.2	7.60	5.0	5.1	10.2	2.8	5.7	3.0	7.4	5.7
Fe_2O_3	68.6	72.3	63.4	77.8	74.4	67.2	87.5	83.4	84.1	64.83	46.5	44.2	59.7	60.2	47.3	46.6	78.2	55.0
MgO	0.2	0.2	0.2	0.1	0.2	0.1	0.1	0.1	0.1	0.13	0.4	0.5	1.0	2.2	0.3	0.5	0.8	0.2
Al_2O_3	10.1	8.8	9.2	6.6	10.1	12.0	4.0	4.4	4.7	0.34	0.6	0.7	0.7	0.2	0.7	4.1	0.4	0.2
TiO_2	4.3	2.3	1.7	0.5	1.6	1.0	1.2	1.4	1.1	0.03	0.3	0.3	0.1	0.1	0.2	0.1	0.2	0.0
Cr_2O_3	0.52	0.46	0.57	0.72	1.39	4.49	1.00	0.33	2.38	0.00	1.11	0.40	0.17	0.42	0.19	0.71	1.15	0.13
MnO	0.62	2.49	0.78	0.00	0.46	0.06	0.36	0.69	0.00	0.33	0.05	0.13	0.14	0.66	0.04	0.03	0.35	0.42
CoO	0.05	0.11	0.04	0.04	0.05	0.04	0.08	0.01	0.00	0.04	0.00	0.03	0.00	0.00	0.00	0.00	0.29	0.00
NiO	0.5	0.6	0.5	1.0	0.5	1.2	1.1	0.3	1.1	2.16	2.5	2.4	2.2	1.1	2.2	1.1	2.4	2.1
Total	84.0	86.6	80.6	81.8	88.0	83.3	88.0	84.3	88.3	69.1	51.9	49.4	68.4	61.8	51.9	51.5	83.4	58.4

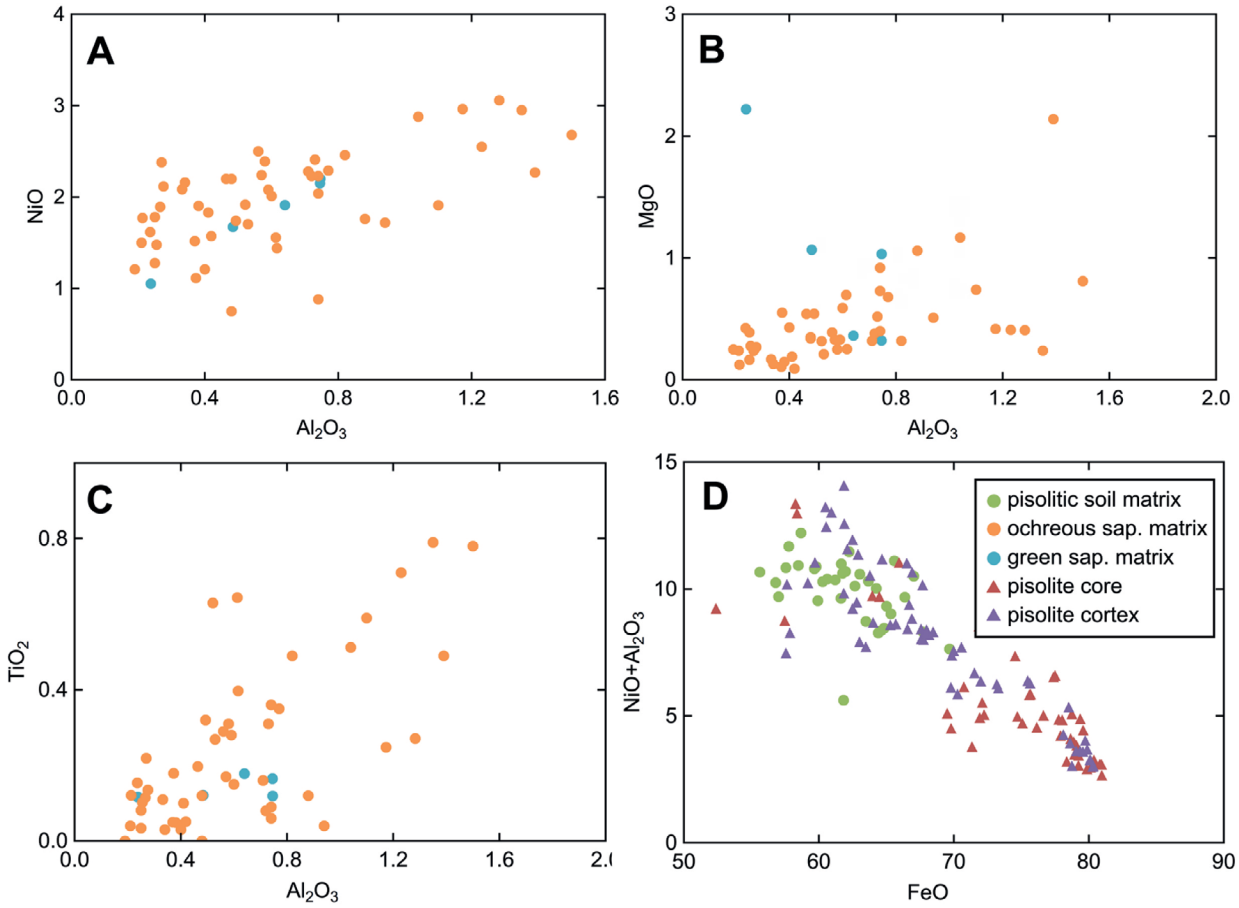

Figure 15. Binary plots showing the mineral chemistry variations of Fe-oxy-hydroxides occurring in the ferruginous matrix and pisolites. Variables are expressed in oxides.

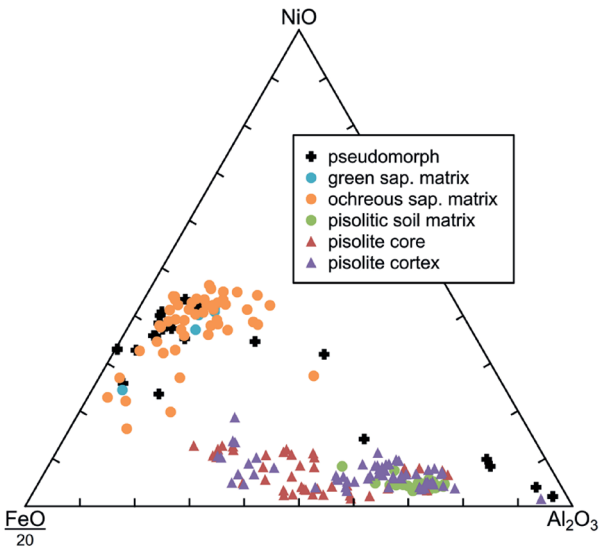

Figure 16. Ternary plot comparing the relative amount of FeO:NiO:Al2O3 among Fe oxides occurrences.

Reconciliation of mineral quantification and bulk Ni mass

The XRPD-Rietveld data, coupled with the corresponding median Ni grades obtained by EMPA in each mineral, incorporating data from Putzolu *et al.* (2021), allowed carrying out the calculation of the Ni deportment (Tab. 5).

In the saprock, serpentine carries approximately 54 wt% of the Ni, while chlorite accounts for 17 wt% Ni. The remaining 29 wt% of Ni occurs in goethite. In the green saprolite, the importance of chlorite as a Ni carrier rises to 29 wt%, serpentines host 34 wt% of Ni, while goethite hosts nearly 36 wt% of the Ni. In the ferruginous saprolite the main host of Ni are chlorites (~46 wt%) (Tab. 5) as its bulk content increases to 17.5 wt% (Fig. 6, Tab. 1) and the total Ni grade increases to 2.8 wt% Ni. Goethite also becomes an important Ni carrier (~39 wt%), due to its abundance (~26 wt%). In the ochreous saprolite, chlorite and Fe-oxy-hydroxides account for respectively 38 wt% and 60 wt% of the bulk Ni. In the pisolitic soil, Ni is contained almost completely in hematite. Despite chromite having only a minor content of Ni, it is responsible for hosting about 10% of the bulk Ni in the pisolitic soil.

DISCUSSION

The lateritic profile of Santa Fé comprises five regolith units with quite different chemical and mineralogical footprints. The basal saprock and overlying green saprolite units are both Mg- and Si-rich and Fe-poor, with Ni-bearing serpentine as the most abundant mineral. These units have a substantial thickness (> 8 m), although the observed Ni grades are generally low. In the saprock, the median Ni grade is 0.22 wt% NiO, with a few drill intercepts showing outlier high Ni grades, probably representing minor fracture-filled green clay

Table 5. Reconciliation and wt% Ni contribution by host mineral (SFPT-050S).

	Upper pisolitic soil	Lower pisolitic soil	Ochreous saprolite	Ferruginous saprolite	Green saprolite	Saprock
wt% Ni	0.3%	0.5%	1.5%	2.8%	2.4%	1.7%
Chromite	10.8%	6.3%	2.1%	1.9%	1.1%	0.7%
Hematite	86%	73%	20%	11%	-	-
Goethite	4%	21%	40%	39%	36%	29%
Chlorite	-	-	38%	46%	29%	17%
Serpentine	-	-	-	2%	34%	54%
Total	100%	100%	100%	100%	100%	100%

veinlets. In the green saprolite Ni grades are higher (0.68% NiO), due to the higher amounts of nickeliferous chlorite. The ferruginous and ochreous saprolite units have a lower thickness than the basal units (about 3 m thick both), but they show the highest Ni grades, with a median of 1.50 and 1.44 wt% Ni, respectively. In these units, the main Ni-bearing minerals are chlorites and Fe-oxy-hydroxides.

Golightly (2010) indicates that in the Santa Fé deposit, the Ni ore in the ferruginous and ochreous saprolites lies entirely within the vertical range of water table fluctuation and, consequently, has little topographic control. The regolith may be divided into two contrasting geochemical environments. One is in the more reduced and saturated zone, and the other, ore bearing, occurs in the oxidized zone exposed to the water table fluctuation, where Fe is precipitated as oxy-hydroxides, as commonly reported in laterite profiles (Nahon and Tardy 1992, Butt and Cluzel 2013). Before discussing the origin of nickeliferous chlorites, it is important to consider that a significant portion of this phyllosilicate formed during a pre-lateritic hydrothermal stage after olivine + pyroxene + Cr-spinels assemblage, leading to the formation of a ferritchromite + amphibole + Fe-Ni(Co)-sulfide + chlorite + silica association (Putzolu *et al.* 2021). During the chromite-to-ferritchromite transformation, the former released Al, which in the presence of Si led to the chlorite formation (Putzolu *et al.* 2021). This resulted in the residual concentration of chlorite and ferritchromite in the regolith. However, primary hydrothermal chlorite alone cannot explain all the chlorite present in the regolith. In the serpentinized dunite, the Al content is very low (med ~ 0.3% Al_2O_3) and part of this Al is also present in pyroxenes and spinels. The Al content in the saprolite are of the order of ~2% Al_2O_3 or more as a result of absolute enrichment as demonstrated by mass balance calculations.

Based on our additional observation, a significant portion of chlorite occurs disseminated in the saprolite fabric and appears unrelated to ferritchromite (no paragenesis). This indicates that a part of the chlorite could be supergene and able to incorporate Ni in order to become the most important single ore mineral in the regolith at Santa Fé.

Three basic mechanisms by which chlorite may be formed by supergene processes in the regolith at Santa Fé were discussed here:

- the solid-state transformation (SST) as described by Beaufort *et al.* (2015), takes place through a cell-preserving phase transition which may be considered as a polymorphic mineral reaction, even though fluids may play an important role as catalysts for the transformation. Beaufort *et al.* (2015) showed that the transformation of berthierine (Al-bearing Fe^{2+}-rich serpentine-group mineral) into ferruginous chlorites is an example of SST reaction and that it may occur in an Fe-rich reduced environment at low temperatures (< 40°C). On the other hand, Cressey *et al.* (2008) have identified clinochlore interstratified throughout lizardite crystals and suggest that an influx of Al causes the nucleation and growth of clinochlore layers at the expense of lizardite layers. Ryan and Reynolds (1997) showed that alteration of serpentine to chlorite takes place in a layer-by-layer basis rather than by dissolution-crystallization (DC) growth;
- Beaufort *et al.* (2015) also showed that smectite (saponite) may transform into Mg-chlorite by DC in a fluid-rich open system environment whereby the resulting chlorite crystals are chemically, structurally, and texturally different from the precursor smectite. Al and Ni are incorporated into this supergene chlorite, but the conversion of saponite to clinochlore predominates in an environment where Fe^{2+} is not available for silicate reactions. In Santa Fé, this may be a feasible mechanism in the lower saprolite zone, where Fe in solution is more limited and conditions are more reducing. However, the amount of smectite in these lower zones have been shown to be very small and, by itself, cannot explain the bulk of the present chlorite;
- the direct precipitation of chlorite from saturated solution (authigenesis), is also possible, especially below the water table where green saprolite and saprock prevail. According to Worden *et al.* (2020), in sandstones, such chlorite may occur as grain-coating, pore-filling or grain-replacing. In Santa Fé, these features have not been observed in the regolith as a result of the supergene process. However, Putzolu *et al.* (2021) have recognized hydrothermal chlorite in silica pores in the saprock, where the alteration is isovolumetric. ln addition, if precipitation in pores did occur in the regolith, the evidence may have been greatly obliterated by fabric re-accommodation.

Therefore, since a component of the chlorite was formed during the pre-lateritic stage (Putzolu *et al.* 2021), we propose that chlorite might also have derived from serpentine alteration via SST transformation with Al influx through the water table. However, more detailed textural and microchemical

investigations are required to understand the precise chemical and mineralogical processes involved. High resolution transmission electron microscopy (HRTEM) analyses are recommended to identify and characterize the potential transition from 7 Å (serpentine) to 14 Å (chlorite) layers, which characterizes this transformation (Banfield and Bailey 1996, Xu and Veblen 1996, Cressey *et al*. 2008, Beaufort *et al*. 2015).

Chlorites may also be subject to supergene alteration. Suárez *et al*. (2011) have identified different types of Mg-phyllosilicate in the Aguablanca regolith, including chlorites that are capable of retaining Ni from weathering solutions. These chlorites may be inherited and partially altered or authigenic. In Santa Fé, chlorites are more enriched in Fe and Ni above the green saprolite, as a result of Ni and Fe incorporation in the region of water table fluctuation. Besides, part of the hydrothermal chlorite could have experienced Al enrichment in comparison to Al-poor chlorites recorded in saprock (Fig. 9B). This would suggest that part of the influx of Al into the saprolite may have been incorporated into the residual hydrothermal chlorites in the regolith.

Across all the regolith units, it is clear that chlorite is a minor component in the saprock. It may occur as a hydrothermal residual phase, but it may also occur locally as a later-stage mineral resulting from serpentine alteration (Fig. 8A). In the saprock, Fe-oxy-hydroxides pseudomorphing olivines are also an important component. These pseudomorphs contain most of the Fe oxy-hydroxides present in the saprock and their Ni contents (1.7 wt% NiO) are distinctly higher than those of the primary Mg-Fe silicate minerals occurring in the bedrock (olivine - 0.35 wt% NiO; serpentine - 0.27 wt% NiO; and pyroxene - 0.17 wt% NiO; Oliveira and Trescases 1980). Despite evidence of Ni remobilization and enrichment in the saprock, mass balance shows only a minor addition of Ni. Therefore, Ni redistribution must have taken place locally, leading to concentrations that are far from reaching a significant ore grade (0.22 wt% NiO).

In the green saprolite, closer to the water table, the availability of Ni in solution would have been higher and serpentine is more unstable. It is believed that most part of supergene nickeliferous chlorite is formed in this unit, at the expense of serpentines resulting in increased Ni grades (0.88% NiO). Hydrothermal chlorite has also experienced supergene overprinting with Ni enrichment. The Al source necessary to form these chlorites may be the regolith profile over pyroxenites or peridotites present within the ultramafic massif. In green saprolite, the amount of goethite increases as it becomes part of a fine ferruginous matrix with a median grade of 0.68 wt% NiO. In this matrix, goethite occurs intermixed with finely disseminated Ni chlorite wisps. The Ni bearing Fe-oxy-hydroxides pseudomorphs are stable and remain an important component, likely representing the poorly crystalline phases indicated by the wide peaks of goethite measured by XRPD. This means that, at the base of the profile, Fe-oxy-hydroxides are still at their early stages of formation (Fig. 8F).

In ferruginous zones, chlorite is still the dominant Ni mineral, but Fe is more strongly incorporated into its structure thereby increasing chlorite stability in the regolith (Oliveira and Melfi 1979). In general, the main mechanism of Ni enrichment in chlorites (and serpentines) is by substitution of Mg for Ni, as often reported in the literature (Foster 1962, Golightly 1981, Brand *et al*. 1998, Gleeson *et al*. 2003, Freyssinet *et al*. 2005). However, we have also identified an inverse association between Ni and Al on EDX maps, indicative of the phenomenon that Al first fills the tetrahedral site and then, consequently, its availability to occupy octahedral site diminishes, allowing Fe and Ni to be incorporated.

Figure 11 shows that the chlorites from the Vermelho deposit (Carajás Province) tend to lose Mg in the transformation from silicate ore zone to the oxide ore zone, but Si is not leached in the same way. Chlorites from Santa Fé are also Mg depleted, but contrary to Vermelho deposit, a Si loss is associated with Ni and Fe enrichment. This may indicate that the Vermelho deposit was formed under a more silica-saturated and higher water table environment in the past. Bernardelli *et al*. (1983) reports that serpentines and chlorites in the protolith of the Vermelho deposit are products of hydrothermal alteration of olivine and pyroxene. Subsequently upon weathering, olivines weather to goethites, and neoformed serpentine and primary serpentine undergo a supergene alteration to vermiculite and chlorite.

In ferruginous saprolite, the instability of serpentine increases and its bulk concentration drops to nearly 5%. The amount of chlorite remains high (17.5 wt%) as it is residually concentrated. However, chlorites are themselves overprinted by the lateritic process, as shown by their Mg and Si depletion coupled with the Ni and Fe enrichment. From ferruginous saprolite upward, hematite becomes more significant (18.7 wt%), but its limited capacity for retaining Ni (Nahon and Tardy 1992, Trivedi and Axe 2001) results in the relatively low Ni grades in the hematite-bearing units (*i.e.,* pisolitic soil; hematite amount = 50 wt%). The Ni released from the dehydration of Ni-bearing goethite into hematite migrates downward in solution and becomes enriched in the saprolite, a process that is well documented in other lateritic profiles worldwide (Golightly 1981, Nahon and Tardy 1992, Carvalho e Silva and Oliveira 1995, Trivedi and Axe 2001).

In the ochreous saprolite, chlorite is less stable showing Ni and Fe enrichment and Al depletion. The amount of chlorite drops to about 10%, raising the content of Ni hosted on Fe-oxy-hydroxides to nearly 60%.

The median Ni grade of the ochreous saprolite matrix is about 2.0 wt% NiO, which is close to the Ni ore grade of the ochreous saprolite as a whole, and the corresponding Al grade in this matrix is 0.6 wt% Al_2O_3. The composition of chlorites from the ochreous saprolite gives results of 7.2 wt% NiO and 8.9 wt% Al_2O_3; therefore, the ratio of NiO over Al_2O_3 in this chlorite is about 0.8. The same ratio calculated for the matrix is 3.33 (2.0/0.6), suggesting that the amount of chlorite in the matrix material, given by the Al_2O_3 content, is not enough to explain all the Ni present in this matrix. This excess Ni is likely to be hosted in the Fe-oxy-hydroxides.

The stronger Ni and Fe enrichment in the chlorites from the ferruginous and ochreous saprolites is due to the higher

availability of these metals in the zone of water table fluctuation, as a result of their downward leaching (Golightly 2010). Therefore, chlorite in the green saprolite under more reducing and neutral conditions is altered to more Fe- and Ni-rich ones in the Fe-rich zones under more oxidizing and acidic conditions.

From the ferruginous saprolite upward, there is increasing textural evidence of mass movement as the presence of detrital chlorite grains distributed in ferruginous matrix. This is interpreted as resulting from collapse and compaction with concomitant mass lateral flux, a process that occurred at its maximum in the pisolitic soil. This process may be compared to what Colin *et al.* (1992) define as parautoctonous in the humid tropical environment of West Africa, and to what Anand and Paine (2002) define as colluvium–eluvium in the semiarid environment of Western Australia.

The Al enrichment observed on EMPA at pisolite rims marks the pisolite formation in the upper portions of the laterite profile, as often reported in other profiles of humid tropical zones (Nahon and Tardy 1992, Trivedi and Axe 2001). The relatively high Ni content of pisolites rims point out that despite the strong ore leaching in the pisolitic soil, a small part of Ni is still incorporated in the cortex during more recent alterations.

The influence of the protolith and geomorphological setting on the ore distribution are also worth mentioning. Nickel mineralization is restricted to areas within the massif that are generally flat, but still nearly 40 m above the regional plain. Moreover, these flat areas are scattered with serpentinized dunite hills. These are features that promote groundwater flow, which coupled with the relatively low Si content of the serpentinized dunites, prevented Si saturation and precipitation of silcrete or smectitic clays at the base of the regolith. This contrasts with other Ni-laterite deposits under arid climates such as São João do Piauí, in Brazil (Carvalho e Silva and Oliveira 1995) and several deposits in Western Australia (Golightly 1981, 2010, Brand *et al.* 1998, Putzolu *et al.* 2020).

However, smectite clays were locally detected by Oliveira and Melfi (1979) and Putzolu *et al.* (2021) over pyroxenites and peridotites restricted to the borders of the complex with no topographic expression, and were related to the alteration of olivine or pyroxene.

Across the boundaries of the peripherical magmatic lithologies, a lateral migration of Ni has probably taken place, resulting in minor Ni mineralization over pyroxenites with smectite and serpentine as the main Ni-bearing mineral. A similar process has been proposed by Melfi (1974), Colin *et al.* (1990) and Carvalho e Silva and Oliveira (1995) for the Barro Alto and Niquelândia deposits, where there is a marked topographic variation over dunitic and pyroxenitic protoliths allowing the lateral Ni migration to areas where the protolith is richer in Si and Al and, therefore, more suitable to the formation of Ni-rich smectites.

In Santa Fé, the mass balance shows that over pyroxenites Al and Ti are depleted only from the ferruginous saprolite upward, while they behave in a conservative way downward (Fig. 5C). This may indicate that the leached Al and Ti from the regolith over the pyroxenitic rocks may have contributed to the enrichment of these elements in the regolith units that formed over the dunite body (Fig. 5). The mass balance model applied in this work assumes Cr immobility, which has been shown to be more reasonable than all other potential immobile element like Fe, Al, or Ti. Furthermore, the data coverage is robust given the large amount of drill holes cores representing a relatively homogeneous protolith and this corroborates the validity of applying mass balance in the area. According to the applied mass balance model, 46 m of protolith have been consumed to produce the present regolith, but just 27.2 m of protolith was enough to supply the Ni present. The equivalent Ni from the remaining 18.8 m of protolith must have been lost by erosion and/or leaching.

Many authors studied the conditions where Al could solubilize in soils. In general Al can migrate in acidified soils (< 5 pH) rich in organic matter compounds (humic substances can dominate the control of pH and dissolved Al). In addition, Al complexes (*e.g.* organic anions) can be soluble in higher pH, between 5-7 (Bache 1986, Cozzarelli *et al.* 1987, Berggren and Mulder 1995, Thomas 1996, Lofts *et al.* 2001, Jansen 2003). Under this pH range, Al may also migrate as colloidal complexes with silica in the groundwater (Schellmann 1994). Cozzarelli *et al.* (1987) showed that groundwater can act as a sink for Al as it is leached from superficial soils under these acidic conditions. They refer to kaolinite as the main Al receptor; however, in Santa Fé, the low availability of Al near the surface prevents significant kaolinite formation, whereas part of chlorite may have formed recently in the more saturated and reduced zone, where more Al is available.

Most of the soil movement is essentially confined within the limits of the ultramafic massif and could not explain the Al enrichment. This enrichment in saprolite over serpentinized dunites is probably due to Al migration from adjacent rocks that are richer in Al, such as weathered pyroxenes of pyroxenites and peridotites from the border complex or maybe even from the Al-silicate rocks that form the basement of the Santa Fé Complex.

It is noteworthy that serpentinized dunites occurring in stable terranes are more suitable for the development of Ni oxide deposits (Brand *et al.* 1998, Elias 2002, Gleeson *et al.* 2003, Freyssinet *et al.* 2005, Butt and Cluzel 2013). This is due to their low Si and Al content, to the relatively steady water table during the formation and evolution of the deposit and to the absence of significant uplift, so that saprolites are poorly developed and all Fe is precipitated as oxy-hydroxides and concentrates most of the mobilized Ni. Santa Fé and Vermelho follow this pattern, which is corroborated by a favorable climate regime.

The great importance of nickeliferous chlorites in Santa Fé and other deposits such as Vermelho and Onça Puma (Carvalho e Silva 1994, Carvalho e Silva and Oliveira 1995,

Golightly 2010) makes it difficult to classify them as garnierite type, clay type or oxide type deposits, as proposed by Golightly (1981), Brand *et al.* (1998), Elias (2002) and Gleeson *et al.* (2003). However, due to the association of Ni to Fe oxy-hydroxides and chlorites in the ferruginous saprolite and to the better development of the oxide-bearing units, these deposits are probably more closely related to the oxide type. The lack of more significant garnierite mineralization in vein filling fractures in the lower portions of Santa Fé is due to the lack of structures in the bedrock that could allow for a stronger and deeper groundwater flow. This may be a function of the relatively stable tectonic setting of the alkaline ultramafic massif.

CONCLUSIONS

The genesis of Santa Fé Ni laterite deposit is associated with the evolution of the *Velhas* geomorphological cycle from the Miocene to Pliocene, following the *Sul Americano* cycle, whose remnant features constitute the silcrete hilltop that surrounds the deposit area. According to the applied mass balance model about 46 m of protolith has been weathered to produce the present regolith, where the Ni mass accumulated represents only a fraction of the Ni present in the precursor protolith. It is suggested that the deposit has been formed in equilibrium with the present day morphoclimatic regime, given that the main Ni ore horizon is associated with a conspicuous ferruginous zone that coincides with the present-day zone of the water table fluctuation.

Chlorite constitutes one of the main ore minerals with Ni grades in the order of 2.9 to 7.2 wt% NiO in the ferruginous zones (ferruginous and ochreous saprolites) and 1.6 to 2.2 wt% NiO in the lower silicate zone (green saprolite and saprock units). The ferruginous zones constitute the main ore units containing the highest amount of nickeliferous chlorite mixed with the Ni-bearing Fe oxy-hydroxides.

Primary chlorite occurs *in situ* in the serpentinized dunite and reworked in the regolith. Its formation is the result of hydrothermal alteration of chromite, which releases the Al necessary to form hydrothermal chlorite. According to the mass balance calculation, in the saprock and saprolites, chlorites are also formed following the further introduction of Al, Ti, and Ni into the weathering system. The formation of supergene chlorite has been interpreted as resulting from serpentine alteration, likely through a SST process. However, the serpentine-to-chlorite transformation proposed in this study needs to be assessed by further research.

Supergene chlorite formation is, presumably, more active in green saprolite, where serpentine becomes unstable and seemingly more effective in terms of Ni enrichment in the ferruginous and ochreous saprolites, where the Ni input from downward percolating solutions is stronger (Fig. 17).

Nickel enrichment is incipient in the saprock where primary chlorite and serpentine I incorporate Ni into their structures. Late-stage nickeliferous serpentine type II is also formed at this stage (Fig. 17). Further weathering of the green saprolite in the presence of Al in solution could lead to chlorite formation after serpentine and overprinting of primary chlorite. In the ferruginous and ochreous saprolites, serpentine is completely broken down, and the dominant mineralogy becomes nickeliferous chlorite and nickeliferous Fe-oxy-hydroxides. Above the saprolites, Ni is highly depleted following the goethite conversion to hematite with its associated Ni loss.

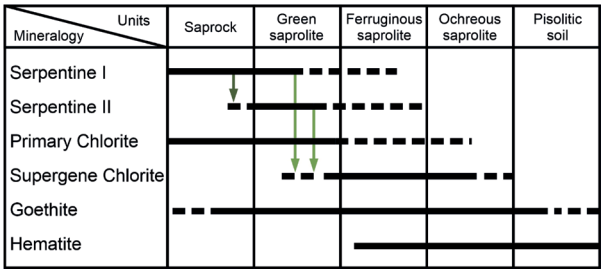

Figure 17. Proposed model of main ore mineral transformation.

Aluminum was introduced into the dunite-derived regolith through the water-table. Primary chlorites may also have been altered by the Al and Ni uptake. It is likely that the source of Al and Ti are the regoliths over the pyroxenite and peridotite that surround the dunite cores of the massif. The main process of Ni enrichment in chlorite is substitution by Mg in the octahedra sites and, depending on the availability of Fe, that may also be incorporated. Chlorites are formed mainly in the silicate zone of the regolith under more reducing and neutral conditions. Upward, ferruginous saprolites chlorites are exposed to a more oxidizing conditions with further Ni enrichment and concomitant depletion of Al^{VI} and Si, especially in the ochreous saprolite. Despite being a subordinate mineral in the ferruginous saprolite, chlorite constitutes the main component of the ore and, together with Fe oxy-hydroxides, constitutes the bulk of the potential Ni ore in Santa Fé.

ACKNOWLEDGMENTS

The first author acknowledges Coordenação de Aperfeiçoamento de Pessoal de Nível Superior (CAPES) for the MSc Scholarship. The Natural History Museum of London is greatly acknowledged for providing access to its microanalytical laboratory to conduct SEM/EMPA work under the skillful assistance of J. Spratt and J. Najorka. This study was also supported by the BEIS Rutherford Fellowship: "Geomicrobiology in Brazil as a tool for innovative biotechnology and capacity building in the mining industry". The authors wish to thank the Centre of Mineral Technology (CETEM) where the XRPD Rietveld characterization was conducted and the Microssonda Lab of the Geology Department of UFRJ for part of the SEM/EMPA analysis. The mining company INVI Ltda. provided access to the deposit and permission to collect and study core samples. C. Porto is thankful for the opportunity to work in the area in charge of the regolith studies and for the permission to use proprietary geochemical data and to publish this paper.

ARTICLE INFORMATION
Manuscript ID: 20200119. Received on: 11/19/2020. Approved on: 07/21/2021
M.L.M. contributed as main writer, data acquisition, XRPD, Rietveld, microprobe and MEV analyses in Brazil, interpretation, and sampling. He produced all figures with support of others; C.G.P. strong contribution all over the text and figures through corrections and suggestions, regarding the experience on the subject studied, he helped in the interpretation and part of data acquisition from the National History Museum. He also revised the manuscript and provided whole-rock chemistry database; L.S. contributed with important text suggestions, and with figure design and data exposure. She was responsible for a lot of good interpretation and discussion, regarding a vast laterite experience. She also revised the manuscript; F.P. made contributions such as important suggestion in the text, and in figure design and data exposure. He was responsible for a lot of good interpretation and discussion. He also revised the manuscript; R.N. provided equipment, support, and interpretation on XRPD, Rietveld, and MEV data; A.C.B.N. contributed assessing the microprobe data treatment and interpretation, also providing part of the database; H.P. has provided some XRPD data from previous research, and interpretation compared to the new data; R.H. provided equipment, support, and interpretation on microprobe and MEV data in the Natural History Museum, as well as financed field trips and sampling.
Competing Interests: The authors declare no competing interests.

REFERENCES

Al-Khirbash S. 2015. Genesis and mineralogical classification of Ni-laterites, Oman Mountains. *Ore Geology Reviews*, **65**(P1):199-212. https://doi.org/10.1016/j.oregeorev.2014.09.022

Almeida F.F.M. 1967. *Origem e Evolução da Plataforma Brasileira*. Brasil: DNPM.

Anand R.R., Paine M. 2002. Regolith geology of the Yilgarn Craton, Western Australia: Implications for exploration. *Australian Journal of Earth Sciences*, **49**(1):3-162. https://doi.org/10.1046/j.1440-0952.2002.00912.x

Bache B.W. 1986. Aluminium mobilization in soils and waters. *Journal of the Geological Society*, **143**(4):699-706. https://doi.org/10.1144/gsjgs.143.4.0699

Banfield J.F., Bailey S.W. 1996. Formation of regularly interstratified serpentine-chlorite minerals by tetrahedral inversion in long-period serpentine polytypes. *American Mineralogist*, **81**(1-2):79-91. https://doi.org/10.2138/am-1996-1-211

Barbour A.P. 1976. *Geologia do Maciço Ultramáfico de Santa Fé, Goiás*. Doctorate Thesis, Universidade de São Paulo, São Paulo, 138 p.

Barbour A.P., Hypolito R. 1983. Geological aspects of lateritization and superficial geology of a mafic-ultramafic alkaline complex in central Brazil. *In*: International Seminar on Lateritisation Processes, 2., 1983, São Paulo. *Annals…*, p. 137–146

Beaufort D., Rigault C., Billon S., Billault V., Inoue A., Inoue S., Patrier P. 2015. Chlorite and chloritization processes through mixed-layer mineral series in low-temperature geological systems – a review. *Clay Minerals*, **50**(4):497-523. http://dx.doi.org/10.1180/claymin.2015.050.4.06

Berger H. 1986. Study of the K alpha emission spectrum of copper. X-Ray Spectrometry, **15**(4):241-243. https://doi.org/10.1002/xrs.1300150405

Berggren D., Mulder J. 1995. The role of organic matter in controlling aluminum solubility in acidic mineral soil horizons. *Geochimica et Cosmochimica Acta*, **59**(20):4167-4180. https://doi.org/10.1016/0016-7037(95)94443-J

Bernardelli A., Melfi A.J., Oliveira S.D., Trescases J.J. 1983. The Carajás nickel deposits. *In*: International Seminar on Lateritisation Processes, 2., 1983. *Annals…*, p. 107-118.

Brand N.W., Butt C.R.M., Elias M. 1998. Nickel laterites: classification and features. *Journal of Australian Geology & Geophysics*, **17**(4):81-88.

Braun O.P.G. 1970. Contribuição à geomorfologia do Brasil Central. *Revista Brasileira de Geografia*, **32**:3-40.

Brod J.A., Barbosa E.S.R., Junqueira-Brod T.C., Gaspar J.C., Diniz-Pinto H.S., Sgarbi P.B.A., Petrinovic I.A. 2005. The Late-Cretaceous Goiás Alkaline Province (Gap), Central Brazil. In: Comin-Chiaramonti P., Gomes C.B. (eds.). *Mesozoic to Cenozoic Alkaline Magmatism in the Brazilian Platform*. São Paulo: Edusp/Fapesp, p. 261-316.

Butt C.R.M., Cluzel D. 2013. Nickel laterite ore deposits: Weathered serpentinites. *Elements*, **9**(2):123-128. https://doi.org/10.2113/gselements.9.2.123

Carvalho e Silva M.L.M. 1994. *Cristaloquímica dos minerais do minério laterítico de níquel: o exemplo do Vermelho, Serra dos Carajás (PA)*. Doctorate Thesis, Universidade de São Paulo, São Paulo, 88 p.

Carvalho e Silva M.L.M. de, Oliveira S.M.B. 1995. As fases portadoras de níquel do minério laterítico de níquel do Vermelho, Serra dos Carajás (PA). *Revista Brasileira de Geociências*, **25**(1):69-78.

Cheary R.W., Coelho A. 1992. A fundamental parameters approach to X-ray line-profile fitting. *Journal of Applied Crystallography*, **25**(2):109-121. https://doi.org/10.1107/S0021889891010804

Colin F., Brimhall G.H., Nahon D., Lewis C.J., Baronnet A., Danti K. 1992. Equatorial rain forest lateritic mantles: a geomembrane filter. *Geology*, **20**(6):523-526. https://doi.org/10.1130/0091-7613(1992)020%3C0523:ERFLMA%3E2.3.CO;2

Colin F., Nahon D., Trescases J.J., Melfi A.J. 1990. Lateritic weathering of pyroxenites at Niquelândia, Goias, Brazil: the supergene behavior of nickel. *Economic Geology*, **85**(5):1010-1023. https://doi.org/10.2113/gsecongeo.85.5.1010

Cozzarelli I.M., Herman J.S., Parnell R.A.J. 1987. The mobilization of aluminum in a natural soil system: effects of hydrologic pathways. *Water Resources Research*, **23**(5):859-874. https://doi.org/10.1029/WR023i005p00859

Cressey G., Cressey B.A., Wicks F.J. 2008. The significance of the aluminium content of a lizardite at the nanoscale: the role of clinochlore as an aluminium sink. *Mineralogical Magazine*, **72**(3):817-825. https://doi.org/10.1180/minmag.2008.072.3.817

Danni J.C.M. 1994. Os picritos alcalinos da região de Iporá: implicações na gênese dos complexos do tipo central do sul de Goiás. *Revista Brasileira de Geociências*, **24**(2):112-119.

Dixon J.B. 1989. Kaolin and serpentine group. *In*: Dixon J.B., Weed S.B. (eds.). *Minerals in Soil Environments*. 2ª ed. Madison: Soil Science Society of America, p. 467-525.

Elias M. 2002. Nickel laterite deposits – geological overview, resources and exploitation. *In*: Cooke D.R., Pongratz J. (eds.). Giant ore deposits: characteristics, genesis and exploration: CODES Special Publication 4. Hobart: University of Tasmania, p. 205-220.

Foster M.D. 1962. Interpretation and a classification of the chlorite. *US Geological Survey Professional Paper*, **414**:1-33.

Freyssinet P., Butt C.R.M., Morris R.C., Piantone P. 2005. Ore-forming processes related to lateritic weathering. *Economic Geology*, 681-722. https://doi.org/10.5382/AV100.21

Gleeson S.A., Butt C.R.M., Elias M. 2003. Nickel laterites: a review. *SEG Newsletter*, **54**:1-48.

Gleeson S.A., Herrington R.J., Durango J., Velásquez C.A., Koll G. 2004. The mineralogy and geochemistry of the Cerro Matoso S. A. Ni laterite

deposit, Montelíbano, Colombia. *Economic Geology*, **99**(6):1197-1213. https://doi.org/10.2113/gsecongeo.99.6.1197

Golightly J.P. 1981. Nickeliferous laterite deposits. *Economic Geology*, 710-735. https://doi.org/10.5382/AV75.18

Golightly J.P. 2010. Progress in understanding the evolution of nickel laterites. *Society of Economic Geologists: Special Publications*, **15**:451-485. https://doi.org/10.5382/SP.15.2.07

Golightly J.P., Arancibia O.N. 1979. The chemical composition and infrared spectrum of nickel-and iron-substituted serpentine from a nickeliferous laterite profile, Soroako, Indonesia. *The Canadian Mineralogist*, **17**(4):719-728.

Grant J.A. 1986. The isocon diagram - a simple solution to Gresens' equation for metasomatic alteration. *Economic Geology*, **81**(8):1976-1982. https://doi.org/10.2113/gsecongeo.81.8.1976

Grant J.A. 2005. Isocon analysis: a brief review of the method and applications. *Physics and Chemistry of the Earth*, **30**(17-18):997-1004. https://doi.org/10.1016/j.pce.2004.11.003

Hölzer G., Fritsch M., Deutsch M., Härtwig J., Förster E. 1997. K alpha1,2 and K beta1,3 X-ray emission lines of the 3d transition metals. *Physical Review A.*, **56**(6):4554-4568. https://doi.org/10.1103/PhysRevA.56.4554

International Centre for Diffraction Data (ICDD). *PDF4+ Relational Powder Diffraction File*. Available at: https://www.icdd.com/pdf-4/. Accessed on: Jan. 15, 2019.

Jansen B. 2003. *The mobility of aluminium, iron and organic matter in acidic*. PhD Thesis, IBED, Universiteit van Amsterdam, 187 p.

King L.C. 1956. A geomorfologia do Brasil Oriental. *Revista Brasileira de Geografia*, **2**:147-265.

Lambiv Dzemua G., Gleeson S.A., Schofield P.F. 2013. Mineralogical characterization of the Nkamouna Co–Mn laterite ore, southeast Cameroon. *Mineralium Deposita*, **48**(2):155-171. https://doi.org/10.1007/s00126-012-0426-3

Lofts S., Woof C., Tipping E., Clarke N., Mulder J. 2001. Modelling pH buffering and aluminium solubility in European forest soils. *European Journal of Soil Science*, **52**(2):189-204. https://doi.org/10.1046/j.1365-2389.2001.00358.x

Melfi A.J. 1974. Características geoquímicas e mineralógicas dos estádios iniciais da alteração superficial das rochas ultrabásicas de Barro Alto (GO). *Boletim IG*, **5**:117-128.

Melfi A.J., Trescases J.J., Oliveira S.M.B. 1979. Les "latérites" nickéliferes du Brésil. *Cah. ORSTOM, Sér. Géol.*, **11**(1):15-42.

Nahon D.B., Tardy Y. 1992. The ferruginous laterites. *In*: Butt C.R.M., Zeegers H. (eds.). *Regolith exploration geochemistry in tropical and subtropical terrains:* Handbook of exploration geochemistry 4. Amsterdam: Elsevier, p. 41-55.

Oliveira S.M.B., Melfi A.J. 1979. Considerações sobre a origem das esmectitas nos níveis de alteração dos piroxenitos de Santa Fé, GO. *Boletim IG*, **10**:91-96.

Oliveira S.M.B., Trescases J.J. 1980. Geoquímica da alteração supérgena das rochas ultramáficas de Santa Fé (Goiás, Brasil). *Revista Brasileira de Geociências*, **10**(4):243-257.

Oliveira S.M.B., Trescases J.J., Melfi A.J. 1992. Lateritic nickel deposits of Brazil. *Mineralium Deposita*, **27**(2):137-146. https://doi.org/10.1007/BF00197099

Paixão M.A.P., Nilson A.A., Dantas E.L. 2008. The neoproterozoic quatipuru ophiolite and the Araguaia fold belt, central-northern Brazil, compared with correlatives in NW Africa. *Geological Society Special Publication*, **294**:297-318. https://doi.org/10.1144/SP294.16

Porto C.G. 2016. Geochemical exploration challenges in the regolith dominated Igarapé Bahia gold deposit, Carajás, Brazil. *Ore Geology Reviews*, **73**(Part 3):432-450. https://doi.org/10.1016/j.oregeorev.2015.10.027

Putzolu F., Abad I., Balassone G., Boni M., Cappelletti P., Graziano S.F., Maczurad M., Mondillo N., Najorka J., Santoro L. 2020. Parent rock and climatic evolution control on the genesis of Ni-bearing clays in Ni-Co laterites: new inferences from the Wingellina deposit (Western Australia). *Ore Geology Reviews*, **120**:103431. https://doi.org/10.1016/j.oregeorev.2020.103431

Putzolu F., Balassone G., Boni M., Maczurad M., Mondillo N., Najorka J., Pirajno F. 2018. Mineralogical association and Ni-Co deportment in the Wingellina oxide-type laterite deposit (Western Australia). *Ore Geology Reviews*, **97**:21-34. https://doi.org/10.1016/j.oregeorev.2018.05.005

Putzolu F., Boni M., Mondillo N., Maczurad M., Pirajno F. 2019. Ni-Co enrichment and High-Tech metals geochemistry in the Wingellina Ni-Co oxide-type laterite deposit (Western Australia). *Journal of Geochemical Exploration*, **196**:282-296. https://doi.org/10.1016/j.gexplo.2018.11.004

Putzolu F., Santoro L., Porto C., Mondillo N., Machado M., Saar De Almeida B., Bastos Neto A.C., Herrington R. 2021. The influence of the magmatic to post-magmatic evolution of the parent rock on the Co deportment in lateritic systems: the example of the Santa Fé Ni-Co deposit (Brazil). *Economic Geology*, **116**(4):837-861. https://doi.org/10.5382/econgeo.4819

Ryan P.C., Reynolds R.C. 1997. The chemical composition of serpentine/chlorite in the Tuscaloosa Formation, United States Gulf Coast: EDX vs. XRD determinations, implications for mineralogic reactions and the origin of anatase. *Clays and Clay Minerals*, **45**(3):339-352. https://doi.org/10.1346/CCMN.1997.0450305

Santos P.S. 1975. Identificação de argilas - difração de raios-x. *In*: Santos P.S. (ed.). *Tecnologia de argilas aplicada às argilas brasileiras*. São Paulo: USP-Edgard Blücher, p. 340.

Schellmann W. 1983. Geochemical principles of lateritic nickel ore formation. *In*: International Seminar on Lateritisation Processes, 2., 1983. *Annals…*, p. 119-135.

Schellmann W. 1994. Geochemical differentiation in laterite and bauxite formation, *Catena*, **21**(2-3):131-143. https://doi.org/10.1016/0341-8162(94)90007-8

Suárez S., Nieto F., Velasco F., Martín F.J. 2011. Serpentine and chlorite as effective Ni-Cu sinks during weathering of the Aguablanca sulphide deposit (SW Spain). TEM evidence for metal-retention mechanisms in sheet silicates. *European Journal of Mineralogy*, **23**(2):179-196. https://doi.org/10.1127/0935-1221/2011/0023-2084

Thomas G.W. 1996. Soil pH and soil acidity. *In*: Sparks D.L., Page A.L., Helmke P.A., Loeppert R.H., Soltanpour P.N., Tabatabai M.A., Johnston C.T., Sumner M.E. (eds.). *Methods of soil analysis:* part 3 chemical methods, 5. Madison: Soil Science Society of America; American Society of Agronomy, p. 475-490. https://doi.org/10.2136/sssabookser5.3.c16

Thorez J. 1975. *Phylossilicates and Clay minerals:* a laboratory handbook for their x-ray diffraction analysis. Dison: Lelotte.

Trivedi P., Axe L. 2001. Ni and Zn sorption to amorphous versus crystalline iron oxides: macroscopic studies. *Journal of Colloid and Interface Science*, **244**(2):221-229. https://doi.org/10.1006/jcis.2001.7970

Velde B., Meunier A. 2008. *The origin of clay minerals in soils and weathered rocks*. Berlin: Springer Science & Business Media.

Wiewióra A., Weiss Z. 1990. Crystallochemical classifications of phyllosilicates based on the unified system of projection of chemical composition: II. The chlorite group. *Clay Minerals*, **25**(1):83-92. https://doi.org/10.1180/claymin.1990.025.1.09

Worden R.H., Griffiths J., Wooldridge L.J., Utley J.E.P., Lawan A.Y., Muhammed D.D., Simon N., Armitage P.J. 2020. Chlorite in sandstones. Earth-Science Reviews, **204**:103105. https://doi.org/10.1016/j.earscirev.2020.103105

Xu H., Veblen D.R. 1996. Interstratification and other reaction microstructures in the chlorite-berthierine series. *Contributions to Mineralogy and Petrology*, **124**(3-4):291-301. https://doi.org/10.1007/s004100050192